

A new paradigm for enriching virtual element methods

E. Artioli*, L. Mascotto†

Abstract

We construct a virtual element method (VEM) based on approximation spaces that are enriched with special singular functions. This enriched VEM is tailored for the approximation of solutions to elliptic problems, which have singularities due to the geometry of the domain. Differently from the traditional extended Galerkin method approach, no partition of unity is employed. Rather, the design of the method hinges upon the special structure of the virtual element spaces. We present a full theoretical analysis of the method, supported by several numerical experiments.

AMS subject classification: 65N12, 65N15, 65N30

Keywords: virtual element methods, extended Galerkin methods, enrichment with singular functions, optimal convergence, polygonal meshes

1 Introduction

The virtual element method (VEM) is a recent generalization of the finite element method (FEM) to very general polygonal/polyhedral meshes; see [10]. Differently from several other polytopal methods, virtual element spaces are designed to mimic properties of the solution to the problem under consideration. This is very much in the spirit of Trefftz methods and renders the VEM extremely similar to the boundary element method-based FEM [36]. Even on standard triangular and tetrahedral meshes, new elements can be constructed.

The design of special virtual element spaces mimicking the continuous problem has been exploited in various occasions. Amongst them, we mention the approximation of solutions to the Stokes equation [15] with exactly divergence free spaces; polyharmonic problems [1, 22] with polyharmonic virtual element spaces; problems with zero right-hand side tackled with Trefftz VEM; see, e.g., [28]; elasticity problems [3, 24] with symmetric stresses inserted in the virtual element spaces; see also [2, 9, 37].

In this paper, we construct special virtual element spaces for the approximation of solutions to elliptic problems, which have singularities due to the geometry of the domain. Our approach falls within the broad family of extended Galerkin methods, such as the extended finite element method (XFEM), see, e.g., [29, 30], and the generalized finite element method (GFEM), see, e.g., [35]. These methods work as follows. Consider an elliptic problem on a polygonal domain with smooth data. The solution to this problem has an a priori known singular behaviour at the vertices of the domain; see, e.g., [26] and the references therein. For this reason, a standard FEM converges to the exact solution suboptimally. In order to cope with this suboptimality, in extended Galerkin methods, the approximation space is enriched with special singular functions. A partition of unity is employed in order to patch the local approximation spaces seamlessly. This enrichment permits to recover an optimal convergence rate of the error of the method.

In [16], the extended finite element setting of [30] is translated into the virtual element one. In particular, local spaces consisting of polynomials plus singular functions are patched with the aid of a virtual partition of unity, in the spirit of [31].

Our approach is different and exploits the structure of virtual element spaces. Instead of inserting the singular functions in the approximation spaces explicitly and patching the local spaces with a partition of unity, we proceed as follows. The singular functions, which are typically added

*Dipartimento di Ingegneria Civile e Ingegneria Informatica, Università di Roma Tor Vergata, 00133 Rome, Italy (artioli@ing.uniroma2.it)

†Fakultät für Mathematik, Universität Wien, 1090 Vienna, Austria (lorenzo.mascotto@univie.ac.at)

to the approximation spaces in extended Galerkin methods, belong to the kernel of the differential operator appearing in the problem under consideration. Such singular functions can be inserted into local virtual element spaces, using the fact that they are defined as solutions to local problems with data in a finite dimensional spaces. By tuning the boundary conditions in local spaces suitably, we include the singular functions implicitly. Eventually, local spaces are patched in a nonconforming fashion.

A first advantage of our approach resides in the flexibility of using polygonal meshes. On the other hand, the analysis and the implementation of the method hinge upon a minor modification of what is done in standard nonconforming VEM; see, e.g., [4]. Furthermore, the structure of nonconforming spaces allows for the use of techniques suited to damp the ill-conditioning, which typically arises in extended Galerkin methods.

The method presented in this paper can be extended to more general problems, such as linear and non linear elasticity problems. The extension to three dimension VEM is straightforward, thanks to the nonconforming structure of the space; see [20].

The enriched virtual element method is based on two main ingredients: local stabilizations and projections onto bulk and face enriched polynomial spaces. We develop the analysis of the method for arbitrary polynomial order.

Structure of the paper. In Section 2, we present the model problem and recall some regularity results for elliptic partial differential equations on polygonal domain: We focus on the case, where the singularities attain at the corner of the domain. We devote Section 3 to the design of the enriched virtual element method. Its theoretical analysis is the topic of Section 4. Here, we also discuss some generalizations of the method. The theoretical results are validated by several numerical experiments in Section 5. We draw some conclusions in Section 6 and provide the implementation details in Appendix A.

Notation. We employ a standard notation for Sobolev spaces. Given $D \subset \mathbb{R}^2$ a domain and $s \in \mathbb{N}$, we denote the standard Sobolev space of integer order s over D by $H^s(D)$. The case $s = 0$ is special: The Sobolev space $H^0(D)$ is the Lebesgue space $L^2(D)$. We endow the Sobolev spaces with the standard inner products and seminorms $(\cdot, \cdot)_{s,D}$ and $|\cdot|_{s,D}$. and denote the Sobolev norm of order s by

$$\|\cdot\|_{s,D}^2 := \sum_{\ell=0}^s \|\cdot\|_{\ell,D}^2.$$

For $s = 1$, it is convenient to write

$$a^D(\cdot, \cdot) := (\cdot, \cdot)_{1,D}.$$

Fractional Sobolev spaces can be defined in several ways. We use the definition of finiteness of the Aronszajn-Gagliardo-Slobodeckij norm; see, e.g., [25] and the references therein. In particular, for any sufficiently smooth v on ∂D , set

$$|v|_{\frac{1}{2},\partial D}^2 := \int_{\partial D} \int_{\partial D} \frac{|v(\xi) - v(\eta)|^2}{|\xi - \eta|^2} d\xi d\eta, \quad \|v\|_{\frac{1}{2},\partial D}^2 := \|v\|_{0,\partial D}^2 + |v|_{\frac{1}{2},\partial D}^2.$$

We define the fractional Sobolev space $H^{\frac{1}{2}}(\partial D)$ as

$$H^{\frac{1}{2}}(\partial D) := \left\{ v \in L^2(\partial D) \text{ such that } \|v\|_{\frac{1}{2},\partial D} \text{ is finite} \right\}.$$

Negative (fractional) Sobolev spaces are defined via duality. In particular, we introduce $H^{-\frac{1}{2}}(\partial D)$ as the dual space of $H^{\frac{1}{2}}(\partial D)$. This space and its norm read

$$H^{-\frac{1}{2}}(\partial D) := (H^{\frac{1}{2}}(\partial D))^*, \quad \|v\|_{-\frac{1}{2},\partial D} := \sup_{\|w\|_{\frac{1}{2},\partial D}=1} (v, w)_{0,\partial D}.$$

2 Model problem and regularity of the solution

Let $\Omega \subset \mathbb{R}^2$ be a polygonal domain, with boundary $\Gamma = \overline{\Gamma_N} \cup \overline{\Gamma_D}$, where Γ_D is a closed set in the topology of Γ and $\Gamma_D \cap \Gamma_N = \emptyset$. Denote the outward normal unit vector of Γ by \mathbf{n}_Ω . Let f be an analytic source term on Ω , and g_D and g_N be piecewise smooth functions on Γ_D and Γ_N , respectively. We allow for slit domains, see Figure 1 (left), and domains with internal cuts (or cracks), see Figure 1 (right).

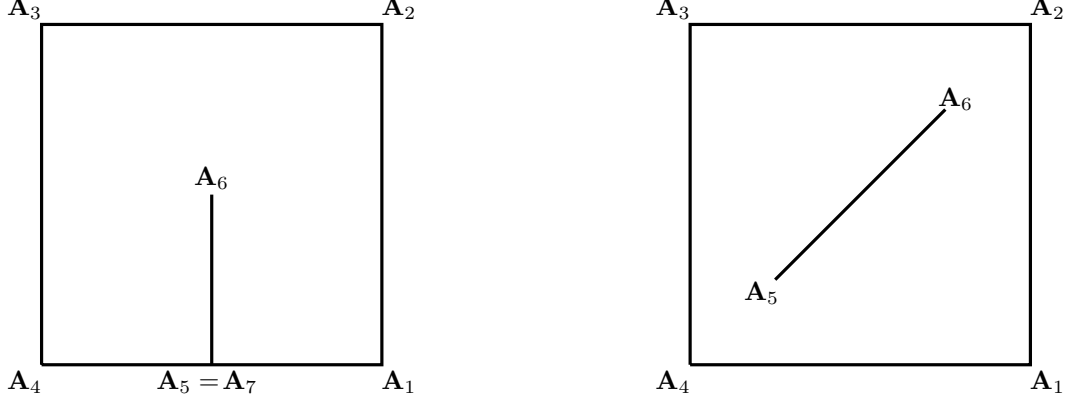


Figure 1: *Left panel:* a slit square domain. *Right panel:* a domain with an internal crack. We highlight the vertices and tips of the domain Ω in bold letters. If a cut starts from the boundary of Ω , then two vertices share the same coordinates.

Consider the following 2D Poisson problem on Ω :

$$\begin{cases} \text{find } u \text{ such that} \\ -\Delta u = f & \text{in } \Omega \\ \mathbf{n}_\Omega \cdot \nabla u = g_N & \text{on } \Gamma_N \\ u = g_D & \text{on } \Gamma_D. \end{cases} \quad (1)$$

Define

$$\begin{aligned} V_{g_D} &:= H_{g_D}^1(\Omega) := \{v \in H^1(\Omega) \mid v = g_D \text{ on } \Gamma_D\}, \\ V_0 &:= H_0^1(\Omega) := \{v \in H^1(\Omega) \mid v = 0 \text{ on } \Gamma_D\}, \\ a(u, v) &= \int_{\Omega} \nabla u \cdot \nabla v \quad \forall u, v \in H^1(\Omega). \end{aligned} \quad (2)$$

In weak formulation, problem (1) reads

$$\begin{cases} \text{find } u \in V_{g_D} \text{ such that} \\ a(u, v) = (f, v)_{0,\Omega} + (g_N, v)_{0,\Gamma_N} \quad \forall v \in V_0. \end{cases} \quad (3)$$

Even if the right-hand side and the boundary conditions g_D and g_N are (piecewise) analytic, the solution u to problem (3) is not analytic over $\overline{\Omega}$ in general. More precisely, u is the combination of an analytic function and a series of singular terms associated with the corners of the domain and the tips of the cracks; see, e.g., [7, 23, 26, 34] and the references therein.

We recall such expansion. Let N_Ω be the number of vertices and of tips of the cracks of Ω . Denote the set of such vertices and tips by $\{\mathbf{A}_i\}_{i=1}^{N_\Omega}$. When no confusion occurs, we call vertex both a vertex and a tip. If a crack has one of the two tips on the boundary of the domain Ω , then two vertices share the same coordinates; see, e.g., the vertices \mathbf{A}_1 and \mathbf{A}_2 in Figure 1 (right). The boundary conditions are imposed on the two lips of the cut separately.

We say that vertex \mathbf{A}_i is a D (N) vertex if $\mathbf{A}_i \in \Gamma_D^\circ$ (Γ_N°). Otherwise, we say that \mathbf{A}_i is a D-N vertex. Introduce the singular exponents

$$\alpha_{i,j} = \begin{cases} j \frac{\pi}{\omega_i} & \text{if } \mathbf{A}_i \text{ is either D or N} \\ (j - \frac{1}{2}) \frac{\pi}{\omega_i} & \text{if } \mathbf{A}_i \text{ is D-N} \end{cases} \quad \forall i = 1, \dots, N_\Omega, \quad j \in \mathbb{N}. \quad (4)$$

To each vertex \mathbf{A}_i , $i = 1, \dots, N_\Omega$, we associate the two (oriented counterclockwise) adjacent edges $\Gamma_{i(1)}$ and $\Gamma_{i(2)}$, and the local set of polar coordinates

$$\mathbf{A}_i \longrightarrow (r_i, \theta_i). \quad (5)$$

Next, we introduce the so-called singular functions. For all $i = 1, \dots, N_\Omega$ and $j \in \mathbb{N}$, if the singular exponent $\alpha_{i,j}$ in (4) does not belong to \mathbb{N} , then we set

$$S_{i,j}(r_i, \theta_i) = \begin{cases} r_i^{\alpha_{i,j}} \sin(\alpha_{i,j} \theta_i) & \text{if } \Gamma_{i(2)} \subset \Gamma_D^\circ \\ r_i^{\alpha_{i,j}} \cos(\alpha_{i,j} \theta_i) & \text{otherwise.} \end{cases} \quad (6)$$

Instead, if $\alpha_{i,j} \in \mathbb{N}$, $i = 1, \dots, N_\Omega$, $j \in \mathbb{N}$, then we set

$$S_{i,j}(r_i, \theta_i) = \begin{cases} r_i^{\alpha_{i,j}} (\log(r_i) \sin(\alpha_{i,j} \theta_i) + \theta_i \cos(\alpha_{i,j} \theta_i)) & \text{if } \Gamma_{i(2)} \subset \Gamma_D^\circ \\ r_i^{\alpha_{i,j}} (\log(r_i) \cos(\alpha_{i,j} \theta_i) + \theta_i \sin(\alpha_{i,j} \theta_i)) & \text{otherwise.} \end{cases} \quad (7)$$

If \mathbf{A}_i is either a D or a N vertex, we can easily check that

$$S_{i,j} \in H^{1+j \frac{\pi}{\omega_i} - \varepsilon}(\Omega) \quad \forall \varepsilon > 0 \quad \text{arbitrarily small.} \quad (8)$$

Moreover, we have

$$\Delta S_{i,j} = 0 \quad \text{pointwise in } \overline{\Omega}.$$

Theorem 2.1. *Let $s > 0$ and assume that $f \in H^{s-1}(\Omega)$ and that g_D and g_N are piecewise in $H^{s+\frac{1}{2}}(\Gamma_D)$ and in $H^{s-\frac{1}{2}}(\Gamma_N)$, respectively. Then, the following decomposition of the solution to problem (3) is valid:*

$$u = u_0 + \sum_{i=1}^{N_\Omega} \sum_{\alpha_{i,j} < s} c_{i,j} S_{i,j}(r_i, \theta_i), \quad (9)$$

where $u_0 \in H^{1+s}(\Omega)$ and $c_{i,j} \in \mathbb{R}$.

Proof. See, e.g., [5, 6] and the references therein. \square

Theorem 2.1 states that, in general, the solution to problem (3) is not analytic, rather has a known singular behaviour at the vertices of the domain and at the tips of the crack. Such singular behaviour depends on the magnitude of the angles, which are associated with the vertices of the domain, regardless of the smoothness of the data.

For ease of presentation, in the remainder of the paper, we assume that u , the solution to problem (3), is such that the series of singular functions in (9) reduces to a single term associated with a single vertex \mathbf{A} . In other words, we assume that u decomposes into

$$u = u_0 + \mathcal{S}_{\mathbf{A}}. \quad (10)$$

In (10), u_0 denotes an analytic function over $\overline{\Omega}$, whereas $\mathcal{S}_{\mathbf{A}}$ is a singular function of the form either (6) or (7), with singularity centred at the corner/tip \mathbf{A} . From (6) and (7), we have that $\mathcal{S}_{\mathbf{A}}(\lambda r, \theta) = \lambda^\alpha \mathcal{S}_{\mathbf{A}}(r, \theta)$, where $\alpha > 0$ depends on $\mathcal{S}_{\mathbf{A}}$ and, consequently, on the geometry of Ω . Additionally, we assume that $\Gamma_N = \emptyset$ and $g_D = 0$ as well; see Remark 1 for further comments on the more general case.

Thus, the problem we aim to solve is

$$\begin{cases} \text{find } u \in V := H_0^1(\Omega) \text{ such that} \\ a(u, v) = (f, v)_{0, \Omega} \quad \forall v \in H_0^1(\Omega). \end{cases} \quad (11)$$

The analysis of this paper can be generalized: In Section 4.8, we discuss how to cope with non-homogeneous boundary conditions; multiple singularities; 3D problems; PDEs characterized by general elliptic operators.

We exhibit a couple of examples that we will be interested in, which fall in the setting of assumption (10).

Example 2.1. Let Ω be the L-shaped domain, see Figure 2 (left),

$$\Omega = (-1, 1)^2 \setminus ([0, 1] \times (-1, 0]). \quad (12)$$

According to (6)-(7), the expected strongest singularity is located at the re-entrant corner $\mathbf{A} = (0, 0)$. Assuming that only Dirichlet boundary conditions are imposed, it is of our interest to consider the case when the singular function is

$$\mathcal{S}_{\mathbf{A}}(r, \theta) = r^{\frac{2}{3}} \sin\left(\frac{2}{3}\theta\right), \quad (13)$$

where (r, θ) are the polar coordinates at \mathbf{A} .

Example 2.2. Let Ω be the unit square with an internal crack, see Figure 2 (right),

$$\Omega = (0, 1)^2 \setminus \{(x, y) \in \mathbb{R}^2 \mid x \in [1/4, 3/4], y = x\}. \quad (14)$$

According to (6)-(7), the expected strongest singularities are located at the two tips of the internal crack. Denote one of the two tips by \mathbf{A} and its polar coordinates by (r, θ) . It is of our interest to consider the case when u is singular at \mathbf{A} only and the singular function is given by

$$\mathcal{S}_{\mathbf{A}}(r, \theta) = r^{\frac{1}{2}} \sin\left(\frac{1}{2}\theta\right).$$

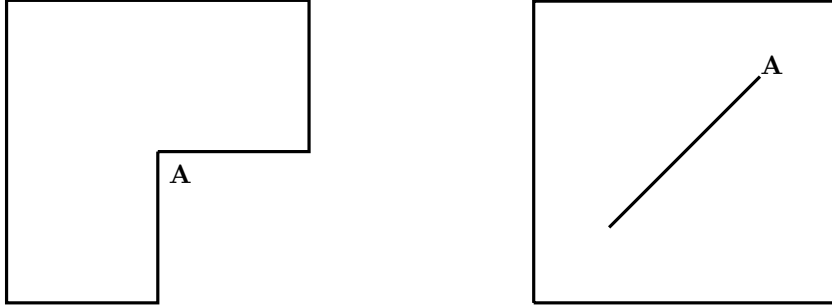


Figure 2: *Left panel:* the L-shaped domain in (12). *Right panel:* the unit square with an internal crack (14). We denote the vertex/tip, where we assume the singularity takes place, by \mathbf{A} .

3 The enriched virtual element method

We devote this section to the design of the novel enriched virtual elements method. To this aim, we introduce sequences of (regular) polygons in Section 3.1. We define the enriched virtual element spaces in Section 3.2, and the discrete bilinear forms and right-hand side in Section 3.3. Eventually, we exhibit the enriched VEM in Section 3.4.

3.1 Regular polygonal decomposition

Here, we introduce the concept of sequences of (regular) polygons and some geometric assumptions.

Consider a sequence $\{\mathcal{T}_n\}_n$ of nonoverlapping polygons partitioning Ω . For all $n \in \mathbb{N}$ and $K \in \mathcal{T}_n$, denote the size of K by h_K , and the mesh size function of \mathcal{T}_n , i.e., the maximum of such local diameter, by h . For each $n \in \mathbb{N}$, denote the set of vertices and edges of \mathcal{T}_n by \mathcal{V}_n and \mathcal{E}_n , and the

set of internal and boundary edges by \mathcal{E}_n^I and \mathcal{E}_n^B , respectively. For all $K \in \mathcal{T}_n$, define \mathcal{E}_n^K its set of edges of the element K and \mathbf{x}_K its centroid. Given $e \in \mathcal{E}_n$ an edge, denote its length by h_e .

Henceforth, we demand that the following assumptions on \mathcal{T}_n , for all $n \in \mathbb{N}$, are valid: There exists a positive constant $\gamma \in (0, 1)$, such that

- (A0) for all couples K_1 and $K_2 \in \mathcal{T}_n$, $\gamma h_{K_1} \leq h_{K_2} \leq \gamma^{-1} h_{K_1}$;
- (A1) for all $K \in \mathcal{T}_n$, K is star-shaped with respect to a ball of radius larger than or equal to γh_K ;
- (A2) for all $e \in \mathcal{E}^K$, the length h_e of e is larger than or equal to γh_K .

We employ assumptions (A0)-(A2) in the analysis of the method; see Section 4 below. Following, e.g., [14, 18, 21], they could be weakened. For the sake of simplicity, we stick here to standard geometric assumptions.

We allow for elements with a crack having (at most) one endpoint on the boundary; see, e.g., the element in the right-upper corner in Figure 4 (left). Nevertheless, we do not consider the case of completely cracked elements. For instance, the central element in Figure 4 (left) is not a square, rather a couple of triangles.

Notation on normal unit vectors. Given $K \in \mathcal{T}_n$, we denote its outward normal unit vector by \mathbf{n}_K . Besides, to each $e \in \mathcal{E}_n$, we associate the normal unit vector \mathbf{n}_e once and for all. In general, \mathbf{n}_e does not coincide with $\mathbf{n}_{K|e}$ necessarily. However, $\mathbf{n}_e \cdot \mathbf{n}_{K|e} = \pm 1$. If $e \in \mathcal{E}_n^B$, then we fix $\mathbf{n}_e := \mathbf{n}_{\Omega|e}$.

3.2 Nonconforming enriched virtual element spaces

The core idea behind the design of the enriched VEM (EVEM) is that the singular functions appearing in the expansions (9) and (10) belong to the kernel of the Laplace operator.

Subdivide \mathcal{T}_n into three layers. The first layer \mathcal{T}_n^1 consists of the polygons abutting or containing the singular vertex \mathbf{A} , as well as polygons that are sufficiently close to \mathbf{A} : given $\tilde{\gamma} > 0$,

$$\mathcal{T}_n^1 := \{K \in \mathcal{T}_n \text{ such that } \text{dist}(\mathbf{A}, \mathbf{x}_K) \leq \tilde{\gamma} \text{diam}(\Omega)\}. \quad (15)$$

Further comments on this definition will be provided in Remark 2 below.

The second layer \mathcal{T}_n^2 consists of the polygons sharing at least one edge with elements in the first layer, i.e.,

$$\mathcal{T}_n^2 := \left\{ K \in \mathcal{T}_n \setminus \mathcal{T}_n^1 \text{ such that there exists } \tilde{K} \in \mathcal{T}_n^1 \text{ with } \text{card}(\mathcal{E}^K \cap \mathcal{E}^{\tilde{K}}) > 0 \right\}.$$

We set the third layer \mathcal{T}_n^3 as the remainder of the elements in \mathcal{T}_n :

$$\mathcal{T}_n^3 := \{K \in \mathcal{T}_n \setminus (\mathcal{T}_n^1 \cup \mathcal{T}_n^2)\}. \quad (16)$$

We consider an analogous splitting for the set of edges \mathcal{E}_n . In particular, we subdivide \mathcal{E}_n into two layers of edges. The first one, \mathcal{E}_n^1 , is the set of all the edges belonging to the boundary of elements in \mathcal{T}_n^1 :

$$\mathcal{E}_n^1 = \{e \in \mathcal{E}_n \text{ such that there exists } K \in \mathcal{T}_n^1 \text{ with } e \subset \partial K\},$$

whereas second layer consists of the remainder of the edges, i.e.,

$$\mathcal{E}_n^2 = \{e \in \mathcal{E}_n \setminus \mathcal{E}_n^1\}.$$

We exhibit a couple of graphical examples of such layers.

Example 3.1. Let Ω be the L-shaped domain split into a Cartesian mesh of 48 elements; see Figure 2 (left). The re-entrant corner is the singular vertex. We show the distributions of elements and edges layers in Figure 3 (left) and (right), respectively. We pick $\tilde{\gamma} = 1/10$ in (15).

Example 3.2. Let Ω be the unit square domain with an internal crack split into a Cartesian mesh of 9 elements; see Figure 2 (right). We top-right tip is the singular vertex. We show the distributions of elements and edges layers, in Figure 4 (left) and (right), respectively. We pick $\tilde{\gamma} = 1/10$ in (15). The upper-right corner contains a crack, which has a tip on the boundary.

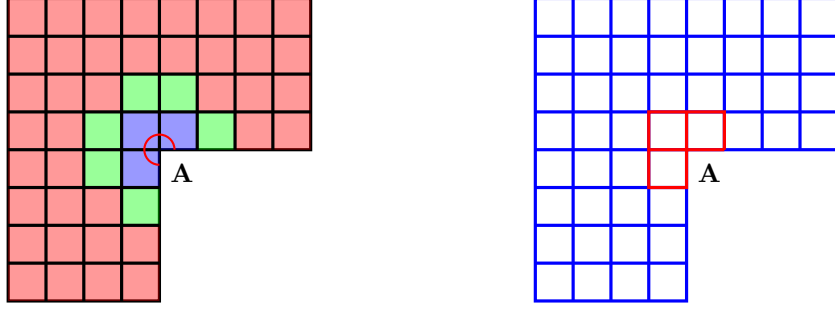


Figure 3: *Left panel:* in blue, the elements in the first element layer \mathcal{T}_n^1 ; in green, the elements in the second element layer \mathcal{T}_n^2 ; in red, the elements in the third layer \mathcal{T}_n^3 . *Right panel:* in red, the edges in the first edge layer \mathcal{E}_n^1 ; in blue, the edges in the second edge layer \mathcal{E}_n^2 . The domain is the L-shaped domain defined in (12). We assume that the solution to problem (11) is singular only at the re-entrant corner **A**. In red, we depict the circumference of radius $1/10$ centred at **A**. The parameter $\tilde{\gamma}$ in (15) is $1/10$.

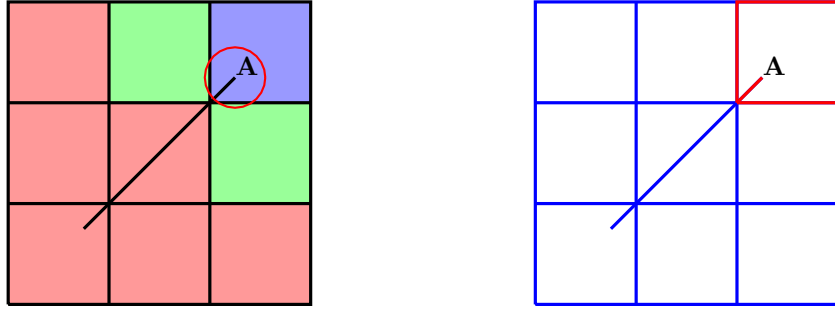


Figure 4: *Left panel:* in blue, the elements in the first element layer \mathcal{T}_n^1 ; in green, the elements in the second element layer \mathcal{T}_n^2 ; in red, the elements in the third layer \mathcal{T}_n^3 . *Right panel:* in red, the edges in the first edge layer \mathcal{E}_n^1 ; in blue, the edges in the second edge layer \mathcal{E}_n^2 . The domain is the unit square domain with an internal crack defined in (14). We assume that the solution to problem (11) is singular only at the right-upper tip of the crack **A**. In red, we depict the circumference of radius $1/10$ centred at **A**. The parameter $\tilde{\gamma}$ in (15) is $1/10$.

Henceforth, we fix a $p \in \mathbb{N}$, which will denote the standard polynomial degree of accuracy of the method, and we introduce auxiliary functions and spaces. Given $K \in \mathcal{T}_n$, define the bulk scaled enriching function

$$\mathcal{S}_{\mathbf{A}}^K(r, \theta) := \mathcal{S}_{\mathbf{A}}\left(\frac{r}{h_K}, \theta\right). \quad (17)$$

For example, if $\mathcal{S}_{\mathbf{A}}$ is given as in (13), then $\mathcal{S}_{\mathbf{A}}^K(r, \theta) = \left(\frac{r}{h_K}\right)^{\frac{2}{3}} \sin\left(\frac{2}{3}\theta\right)$.

Given $e \in \mathcal{E}^K$, define the edge scaled enriching function

$$\mathcal{S}_{\mathbf{A}}^e(r, \theta) := \mathcal{S}_{\mathbf{A}}\left(\frac{r}{h_e}, \theta\right). \quad (18)$$

For example, if $\mathcal{S}_{\mathbf{A}}$ is given as in (13), then $\mathcal{S}_{\mathbf{A}}^e(r, \theta) = \left(\frac{r}{h_e}\right)^{\frac{2}{3}} \sin\left(\frac{2}{3}\theta\right)$.

Note that

$$\mathcal{S}_{\mathbf{A}}^K(r, \theta) = \left(\frac{h_e}{h_K}\right)^{\alpha} \mathcal{S}_{\mathbf{A}}^e(r, \theta), \quad (19)$$

where $\alpha > 0$ depends on the definition of $\mathcal{S}_{\mathbf{A}}$. For example, if $\mathcal{S}_{\mathbf{A}}$ is given as in (13), then $\alpha = 2/3$.

We define the set of enriched polynomials over an element $K \in \mathcal{T}_n$ as follows:

$$\tilde{\mathbb{P}}_p(K) = \begin{cases} \mathbb{P}_p(K) \oplus \mathcal{S}_{\mathbf{A}}^K & \text{if } K \in \mathcal{T}_n^1 \\ \mathbb{P}_p(K) & \text{otherwise.} \end{cases}$$

In other words, on the elements close to the singular vertex/tip \mathbf{A} , we add the singular function $\mathcal{S}_{\mathbf{A}}$ to the standard polynomial space $\mathbb{P}_p(K)$.

Further, we define the set of enriched polynomials over edges:

$$\tilde{\mathbb{P}}_{p-1}(e) = \begin{cases} \mathbb{P}_{p-1}(e) \oplus (\mathbf{n}_e \cdot \nabla \mathcal{S}_{\mathbf{A}|e}^e) & \text{if } K \in \mathcal{E}_n^1 \\ \mathbb{P}_{p-1}(e) & \text{otherwise.} \end{cases}$$

In other words, we consider standard one dimensional polynomial spaces $\mathbb{P}_{p-1}(e)$ on all the edges, with the exception of those belonging to the boundary of the elements in the first layer \mathcal{T}_n^1 . Here, we consider the normal derivative of the scaled enriching function $\mathcal{S}_{\mathbf{A}}^e$ as additional special function.

Next, we define the local enriched virtual element spaces: For all $K \in \mathcal{T}_n$,

$$V_n(K) := \left\{ v_n \in H^1(K) \mid \Delta v_n \in \mathbb{P}_{p-2}(K), \mathbf{n}_e \cdot \nabla v_n|_e \in \tilde{\mathbb{P}}_{p-1}(e) \quad \forall e \in \mathcal{E}^K \right\}. \quad (20)$$

The functions in $V_n(K)$ are unknown in closed-form both in the bulk and the boundary of the element K . This is the reason why the functions are referred to as virtual. The space $V_n(K)$ contains the space of the polynomials of degree p . Furthermore, if $K \in \mathcal{T}_n^1$, then the singular function $\mathcal{S}_{\mathbf{A}}$ belongs to $V_n(K)$ as well. This is the reason why we regard the space $V_n(K)$ as enriched.

We introduce additional notation. Let $\{m_\alpha\}_{|\alpha|=0}^{\dim(\mathbb{P}_{p-2}(K))}$ be a basis of $\mathbb{P}_{p-2}(K)$. For instance, this basis consists of the monomials introduced in [10] or some orthogonal basis as in [27]. We assume that m_α is invariant with respect to homothetic transformations and translations with respect to the barycenter of the element. Besides, let $\{\tilde{m}_\alpha^e\}_{\alpha=0}^{p-1}(e)$ be a basis of $\tilde{\mathbb{P}}_{p-1}(e)$ for all edges $e \in \mathcal{E}^K$. A possible (and robust) choice of the basis is provided by the first $p-1$ Legendre polynomials on the local system of coordinates over e , and the global normal derivative of the singular function $\mathcal{S}_{\mathbf{A}}^e$ over the edge e . More details on enriched polynomial basis functions are given in Section 5 and in Appendix A below.

Consider the following set of linear functionals on $V_n(K)$: For all $v_n \in V_n(K)$,

- the internal moments:

$$\frac{1}{|K|} \int_K v_n m_\alpha \quad \forall \alpha = 1, \dots, \dim(\mathbb{P}_{p-2}(K)); \quad (21)$$

- if $e \in \mathcal{E}_n^1$, the edge moments:

$$\begin{cases} \frac{1}{|e|} \int_e v_n \tilde{m}_\alpha^e & \forall \alpha = 0, \dots, p-1, \forall e \in \mathcal{E}^K, \\ \int_e v_n (\mathbf{n}_e \cdot \nabla \mathcal{S}_{\mathbf{A}}^e)|_e & \alpha = p, \forall e \in \mathcal{E}^K. \end{cases} \quad (22)$$

If $e \in \mathcal{E}_n^2$, then the edge moments are the same, but there is no special moment for $\alpha = p$.

Lemma 3.1. *For all $K \in \mathcal{T}_n$, the set of linear functionals in (21)-(22) is a unisolvent set of degrees of freedom for the space $V_n(K)$.*

Proof. The dimension of $V_n(K)$ is equal to the number of linear functionals; see [4]. Thence, it suffices to prove the unisolvency of such functionals. Observe that

$$|v_n|_{1,K}^2 = - \int_K \underbrace{\Delta v_n}_{\in \mathbb{P}_{p-2}(K)} v_n + \sum_{e \in \mathcal{E}^K} \int_e \underbrace{\mathbf{n}_K \cdot \nabla v_n}_{\in \tilde{\mathbb{P}}_{p-1}(e)} v_n.$$

The first and second terms are zero, for the internal (21) and the edge moments (22) are zero by assumption, respectively. Hence, v_n is constant. This and the fact that its average over ∂K is equal zero entail the assertion. \square

Compared to the degrees of freedom (dofs) in the standard nonconforming VEM [4], we consider the same degrees internal dofs (21). As for the edge dofs (22), we cope with additional moments related to the special functions on the edges of the elements in the first edge layer \mathcal{E}_n^1 .

For future convenience, introduce the local canonical basis $\{\varphi_i\}_{i=1}^{\dim(V_n(K))}$:

$$\text{dof}_j(\varphi_i) = \delta_{i,j}, \quad (23)$$

where $\delta_{i,j}$ denotes the Kronecker delta.

Next, split the bilinear form $a(\cdot, \cdot)$ defined in (2) into local contributions:

$$a(u, v) = \sum_{K \in \mathcal{T}_n} a^K(u, v) := \sum_{K \in \mathcal{T}_n} \int_K \nabla u|_K \cdot \nabla v|_K \quad \forall u, v \in H^1(\Omega).$$

The definition of the degrees of freedom allows us to compute the enriched H^1 -orthogonal projection $\tilde{\Pi}_p^{\nabla, K} : V_n(K) \rightarrow \tilde{\mathbb{P}}_p(K)$:

$$\begin{cases} a^K(v_n - \tilde{\Pi}_p^{\nabla, K} v_n, q_p) = 0 \\ \int_{\partial K} (v_n - \tilde{\Pi}_p^{\nabla, K} v_n) = 0 \end{cases} \quad \forall v_n \in V_n(K), \quad \forall q_p \in \tilde{\mathbb{P}}_p(K). \quad (24)$$

In fact, an integration by parts yields

$$a^K(v_n, q_p) = \underbrace{(v_n, -\Delta q_p)_{0,K}}_{\in \mathbb{P}_{p-2}(K)} + \sum_{e \in \mathcal{E}^K} \underbrace{(v_n, \mathbf{n}_K \cdot \nabla q_p)_{0,e}}_{\in \tilde{\mathbb{P}}_{p-1}(e)}. \quad (25)$$

The first and second term on the right-hand side of (25) are computable from (21) and (22), respectively. The second term can be approximated at any precision by a one dimensional quadrature formula; see Remark 5 below for more comments on this point. For all the elements $K \in \mathcal{T}_n^1$, the projection $\tilde{\Pi}_p^{\nabla, K}$ maps functions belonging to the virtual element space into the space of bulk enriched polynomial spaces $\tilde{\mathbb{P}}_{p-2}(K)$.

Further, for all $e \in \mathcal{E}_n$, we consider the (possibly) enriched L^2 edge projector $\tilde{\Pi}_{p-1}^{0,e} : V_n(K)|_e \rightarrow \tilde{\mathbb{P}}_{p-1}(e)$, defined as

$$\int_e (v_n - \tilde{\Pi}_{p-1}^{0,e} v_n) \tilde{m}_\alpha^e = 0 \quad \forall v_n \in V_n(K), \quad \forall \tilde{m}_\alpha^e \in \tilde{\mathbb{P}}_{p-1}(e). \quad (26)$$

The computability of such projector follows from the definition of the edge degrees of freedom (22).

Eventually, we define the nonenriched L^2 -bulk orthogonal projector $\Pi_{p-2}^{0,K} : V_n(K) \rightarrow \mathbb{P}_{p-2}(K)$ as

$$(v_n - \Pi_{p-2}^{0,K} v_n, q_{p-2})_{0,K} = 0 \quad \forall q_{p-2} \in \mathbb{P}_{p-2}(K). \quad (27)$$

The projector $\Pi_{p-2}^{0,K}$ is computable from the internal degrees of freedom (21) and is used for the approximation of the Neumann boundary conditions only; see Remark 1 below.

Next, we define the global nonconforming virtual element space V_n . Given an internal edge $e \in \mathcal{E}_n^I$, denote its two adjacent edges by K^+ and K^- . Moreover, denote the space of $L^2(\Omega)$ functions piecewise in H^1 over \mathcal{T}_n by $H^1(\mathcal{T}_n)$, and define the broken Sobolev norm

$$|v|_{1,\mathcal{T}_n}^2 := \sum_{K \in \mathcal{T}_n} |v_K|_{1,K}^2 \quad \forall v \in H^1(\mathcal{T}_n).$$

Introduce the jump operator across an edge $e \in \mathcal{E}_n^1$: Given $v \in H^1(\mathcal{T}_n)$, set

$$[v]_e = \llbracket v \rrbracket := \begin{cases} v|_{K^+} \mathbf{n}_{K^+} + v|_{K^-} \mathbf{n}_{K^-} & \text{if } e \in \mathcal{E}_n^I \\ v \mathbf{n}_\Omega & \text{if } e \in \mathcal{E}_n^B. \end{cases} \quad (28)$$

Introduce the global nonconforming Sobolev space of order p , subordinated to the mesh \mathcal{T}_n , including homogeneous boundary conditions in a nonconforming sense:

$$H_0^{1,nc}(\mathcal{T}_n, p) := \left\{ v \in H^1(\mathcal{T}_n) \left| \begin{aligned} \int_e \llbracket v \rrbracket \cdot \mathbf{n}_e \tilde{m}_\alpha^e &= 0 \quad \forall \tilde{m}_\alpha^e \in \tilde{\mathbb{P}}_{p-1}(e), \forall e \in \mathcal{E}_n^I; \\ \int_e \llbracket v \rrbracket \cdot \mathbf{n}_\Omega \tilde{m}_\alpha^e &= 0 \quad \forall \tilde{m}_\alpha^e \in \tilde{\mathbb{P}}_{p-1}(e), \forall e \in \mathcal{E}_n^B \end{aligned} \right. \right\}.$$

We define the global test and trial nonconforming enriched virtual element spaces as

$$V_n := \left\{ v_n \in H_0^{1,nc}(\mathcal{T}_n, p) \mid v_n|_K \in V_n(K) \quad \forall K \in \mathcal{T}_n \right\}. \quad (29)$$

We construct the space V_n by a nonconforming coupling of the local edge degrees of freedom (22). The global canonical basis is defined from its local counterparts (23) accordingly.

3.3 The discrete bilinear form and right-hand side

The functions in the virtual element spaces are not available in closed-form. Thus, in order to design the numerical scheme for the approximation of solutions to (11), we introduce a global bilinear form and a right-hand side that are computable in terms of the degrees of freedom. To this purpose, we generalize the construction in [4] to the enriched setting.

The discrete bilinear form. Using the orthogonality property of the projector $\tilde{\Pi}_p^{\nabla, K}$ in (24), we apply the Pythagoras' theorem in Hilbert spaces and get

$$a^K(u, v) = a^K(\tilde{\Pi}_p^{\nabla, K} u, \tilde{\Pi}_p^{\nabla, K} v) + a^K((I - \tilde{\Pi}_p^{\nabla, K})u, (I - \tilde{\Pi}_p^{\nabla, K})v) \quad \forall u, v \in H^1(K).$$

The first term on the right-hand side is computable on $V_n(K) \times V_n(K)$, see (25), whereas the second one is not. Following the virtual element gospel [10, 11], we introduce any symmetric bilinear form $S^K : \ker(\tilde{\Pi}_p^{\nabla, K}) \times \ker(\tilde{\Pi}_p^{\nabla, K}) \rightarrow \mathbb{R}$ satisfying

$$c_*(K)|v_n|_{1,K}^2 \leq S^K(v_n, v_n) \leq c^*(K)|v_n|_{1,K}^2 \quad \forall v_n \in V_n(K), \quad \forall K \in \mathcal{T}_n. \quad (30)$$

In (30), $c_*(K)$ and $c^*(K)$ are two positive constants, possibly depending on the polynomial degree p , the geometric properties of K , and the singular function $\mathcal{S}_\mathbf{A}$.

Having this at hand, define the local discrete bilinear forms

$$a_n^K(u_n, v_n) = a^K(\tilde{\Pi}_p^{\nabla, K} u_n, \tilde{\Pi}_p^{\nabla, K} v_n) + S^K((I - \tilde{\Pi}_p^{\nabla, K})u_n, (I - \tilde{\Pi}_p^{\nabla, K})v_n) \quad \forall u_n, v_n \in V_n(K),$$

and the global discrete bilinear form

$$a_n(u_n, v_n) = \sum_{K \in \mathcal{T}_n} a_n^K(u_n|_K, v_n|_K) \quad \forall u_n, v_n \in V_n.$$

We postpone explicit choices and further considerations about the stabilization forms S^K to Section 4.6 below.

For all $K \in \mathcal{T}_n$, the local discrete bilinear forms a_n^K are coercive and continuous with respect to the H^1 seminorm, with coercivity and continuity constants

$$\alpha_*(K) = \min(1, c_*(K)), \quad \alpha^*(K) = \max(1, c^*(K)).$$

In other words, for all $K \in \mathcal{T}_n$, we have

$$\alpha_*(K)|v_n|_{1,K}^2 \leq a_n^K(v_n, v_n) \leq \alpha^*(K)|v_n|_{1,K}^2 \quad \forall v_n \in V_n(K). \quad (31)$$

Moreover, the stabilization is symmetric and polynomially-enriched consistent: For all $K \in \mathcal{T}_n$,

$$a_n^K(q_p, v_n) = a^K(q_p, v_n) \quad \forall q_p \in \tilde{\mathbb{P}}_p(K), \quad \forall v_n \in V_n. \quad (32)$$

The discrete right-hand side. Denote the number and the set of vertices of the element K by N_V and $\{\nu_i\}_{i=1}^{N_V}$, recall the projector $\Pi_{p-2}^{0,K}$ in (27), and define

$$\langle f, v_n \rangle_n = \sum_{K \in \mathcal{T}_n} \langle f|_K, v_n|_K \rangle_{n,K} := \begin{cases} \sum_{K \in \mathcal{T}_n} \int_K f|_K \Pi_{p-2}^{0,K} v_n|_K & \text{if } p \geq 2 \\ \sum_{K \in \mathcal{T}_n} \int_K f|_K (\sum_{i=1}^{N_V} v_n(\nu_i)) & \text{if } p = 1. \end{cases}$$

3.4 The method

The nonconforming enriched virtual element method for problem (11) reads

$$\begin{cases} \text{find } u_n \in V_n \text{ such that} \\ a_n(u_n, v_n) = \langle f, v_n \rangle_n \quad \forall v_n \in V_n. \end{cases} \quad (33)$$

The method (33) is well posed thanks to the continuity and coercivity properties detailed in Section 3.3. We devote Section 4 below to the analysis of (33), whereas we provide the implementation details in Appendix A.

Remark 1. The case of a nonhomogeneous Neumann boundary condition g_N in (3) is dealt with as follows. Dirichlet boundary conditions are enforced in a standard way in the trial and test spaces. As for the approximation of the Neumann boundary condition term, we consider the following approximation:

$$\int_{\Gamma_N} g_N \tilde{\Pi}_{p-1}^{0,e} v_n. \quad (34)$$

4 Error analysis

In this section, we analyse the rate of convergence of the method (33). We present an abstract error result in Section 4.1. In Sections 4.2 and 4.3, we describe the approximation properties of enriched polynomial and enriched virtual element spaces, respectively. On the other hand, Sections 4.4 and 4.5 deal with the approximation of the variational crimes perpetrated in the approximation of the right-hand side and the nonconformity of the method. After introducing and analysing possible stabilizations in Section 4.6, we collect all the above estimates in Section 4.7. We discuss some extensions and generalization in Section 4.8.

4.1 Abstract error analysis

Here, we present the abstract error analysis result for the method (33). Recall that the jump operator $[\![\cdot]\!]_e$ across the edge e is defined in (28), and define the bilinear form $\mathcal{N}_n : H^1(\Omega) \times H_0^{1,nc}(\mathcal{T}_n, p) \rightarrow \mathbb{R}$ as

$$\mathcal{N}_n(u, v) = \sum_{e \in \mathcal{E}_n} \int_e \nabla u \cdot [\![v]\!]_e. \quad (35)$$

Theorem 4.1. *Let u and u_n be the solutions to (11) and (33), respectively. Recall that $\alpha_*(K)$ and $\alpha^*(K)$ are the stability constants in (31), and \mathcal{N}_n is defined in (35). Then, the following a priori estimate is valid: For all u_π piecewise in $\tilde{\mathbb{P}}_p(K)$ and for all $u_I \in V_n$,*

$$\begin{aligned} |u - u_n|_{1, \mathcal{T}_n} \leq \max_{K \in \mathcal{T}_n} \alpha_*^{-1}(K) & \left\{ \sup_{v_n \in V_n} \frac{\langle f, v_n \rangle_n - (f, v_n)_{0, \Omega}}{|v_n|_{1, \mathcal{T}_n}} + \sup_{v_n \in V_n} \frac{\mathcal{N}_n(u, v_n)}{|v_n|_{1, \mathcal{T}_n}} \right. \\ & \left. + \left(1 + \max_{K \in \mathcal{T}_n} \alpha^*(K) \right) (|u - u_\pi|_{1, \mathcal{T}_n} + |u - u_I|_{1, \mathcal{T}_n}) \right\}. \end{aligned} \quad (36)$$

Proof. The proof follows along the same lines as that in [4, Theorem 4.1]. For the sake of completeness, we carry out all the details.

For all $u_I \in V_n$, the triangle inequality entails

$$|u - u_n|_{1, \mathcal{T}_n} \leq |u - u_I|_{1, \mathcal{T}_n} + |u_I - u_n|_{1, \mathcal{T}_n} =: |u - u_I|_{1, \mathcal{T}_n} + |\delta_n|_{1, \mathcal{T}_n}. \quad (37)$$

We estimate the second term on the right-hand side: For all u_π piecewise in $\widetilde{\mathbb{P}}_p(K)$, apply (31) and (32) and get

$$\begin{aligned} |\delta_n|_{1,\mathcal{T}_n}^2 &= \sum_{K \in \mathcal{T}_n} |\delta_n|_{1,\mathcal{T}_n}^2 \leq \sum_{E \in \mathcal{T}_n} \alpha_*^{-1}(K) a_n^K(\delta_n, \delta_n) \\ &\leq \max_{K \in \mathcal{T}_n} \alpha_*^{-1}(K) \sum_{K \in \mathcal{T}_n} \{a_n^K(u_n, \delta_n) - a_n^K(u_I - u_\pi) - a^K(u_\pi - u, \delta_n) - a^K(u, \delta_n)\}. \end{aligned}$$

Observe that

$$\begin{aligned} \sum_{K \in \mathcal{T}_n} a^K(u, \delta_n) &= \sum_{K \in \mathcal{T}_n} \left\{ \int_K -\Delta u \delta_n + \int_{\partial K} \mathbf{n}_K \cdot \nabla u \delta_n \right\} \\ &= (f, \delta_n)_{0,\Omega} + \sum_{e \in \mathcal{E}_n} \int_e \nabla u \cdot \llbracket \delta_n \rrbracket =: (f, \delta_n)_{0,\Omega} + \mathcal{N}_n(u, \delta_n). \end{aligned}$$

Deduce that

$$\begin{aligned} |\delta_n|_{1,\mathcal{T}_n}^2 &\leq \max_{K \in \mathcal{T}_n} \alpha_*^{-1}(K) \left\{ \langle f, \delta_n \rangle_n - (f, \delta_n)_{0,\Omega} - \mathcal{N}_n(u, \delta_n) \right. \\ &\quad \left. + \max_{K \in \mathcal{T}_n} \alpha^*(K) |u_I - u_\pi|_{1,\mathcal{T}_n} |\delta_n|_{1,\mathcal{T}_n} + |u - u_\pi|_{1,\mathcal{T}_n} |\delta_n|_{1,\mathcal{T}_n} \right\}, \end{aligned}$$

which implies

$$\begin{aligned} |\delta_n|_{1,\mathcal{T}_n} &\leq \max_{K \in \mathcal{T}_n} \alpha_*^{-1}(K) \left\{ \frac{\langle f, \delta_n \rangle_n - (f, \delta_n)_{0,\Omega} - \mathcal{N}_n(u, \delta_n)}{|\delta_n|_{1,\mathcal{T}_n}} - \frac{\mathcal{N}_n(u, \delta_n)}{|\delta_n|_{1,\delta_n}} \right. \\ &\quad \left. + (1 + \max_{K \in \mathcal{T}_n} \alpha^*(K)) |u - u_\pi|_{1,\mathcal{T}_n} + \max_{K \in \mathcal{T}_n} \alpha^*(K) |u - u_I|_{1,\mathcal{T}_n} \right\}. \end{aligned}$$

This, together with (37), entails the assertion. \square

4.2 Best enriched polynomial approximation estimates

Given u_π piecewise in $\widetilde{\mathbb{P}}_p(K)$, we show how to estimate from above the term $|u - u_\pi|_{1,\mathcal{T}_n}$ on the right-hand side of (36).

Lemma 4.2. *Let u be the solution to problem (11), u_0 be as in (10), and the assumptions **(A0)**-**(A2)** be valid. Then, there exists u_π piecewise in $\mathbb{P}_p(K)$ such that*

$$|u - u_\pi|_{1,\mathcal{T}_n} \leq ch^p \left\{ \left(\sum_{K \in \mathcal{T}_n^1} |u_0|_{p+1,K}^2 \right)^{\frac{1}{2}} + \left(\sum_{K \in \mathcal{T}_n^2 \cup \mathcal{T}_n^3} |u|_{p+1,K}^2 \right)^{\frac{1}{2}} \right\},$$

where c is a positive constant depending on p and γ , being γ introduced in **(A0)**-**(A2)**, but is independent of h and u .

Proof. For all $K \notin \mathcal{T}_n^1$, we have $\widetilde{\mathbb{P}}_p(K) = \mathbb{P}_p(K)$. Therefore, we pick u_π as the best piecewise $H^1(K)$ polynomial approximant of u . Deduce that

$$|u - u_\pi|_{1,K} = \inf_{q_p \in \mathbb{P}_p(K)} |u - q_p|_{1,K} \leq ch_K^p |u|_{p+1,K}. \quad (38)$$

This is a consequence of standard polynomial best approximation estimates, see, e.g. [17], and the smoothness of u on all $K \notin \mathcal{T}_n^1$. The constant c depends on the degree of accuracy of the method p and on the shape of the element K .

If $K \in \mathcal{T}_n^1$, then, $\widetilde{\mathbb{P}}_p(K) \supsetneq \mathbb{P}_p(K)$: The former space is spanned by the latter *plus* the singular function \mathcal{S}_A^K . Thus, a suitable choice of u_π is given by a combination of the singular function \mathcal{S}_A^K

and the best $H^1(K)$ polynomial approximant of u_0 , being u_0 introduced in (10). This entails, for some constants $\tilde{c} \in \mathbb{R}$,

$$|u - u_\pi|_{1,K} = \inf_{q_p \in \mathbb{P}_p(K)} |u_0 - q_p + \tilde{c}\mathcal{S}_{\mathbf{A}}^K - \tilde{c}\mathcal{S}_{\mathbf{A}}^K|_{1,K} \leq ch_K^p |u_0|_{p-1,K}, \quad (39)$$

where c is a positive constant depending on p and on γ , being γ introduced in (A0)-(A2), but is independent of h and u .

The bound (39) is a consequence of standard polynomial best approximation estimates, see, e.g., [17], and the smoothness of u_0 on all $K \in \mathcal{T}_n^1$. Collecting the local estimates (38) and (39) and summing up over all the elements, we get the assertion. \square

The name of the game in Lemma 4.2 is that the singular part of the solution is approximated by the singular function in the virtual element spaces on the elements close or containing the singular vertex.

4.3 Best interpolation estimates

Here, we show how to estimate from above the term $|u - u_I|_{1,\mathcal{T}_n}$ on the right-hand side of (36), being u_I a generic function in V_n . In particular, we prove an upper bound on the best interpolation error in nonconforming enriched virtual element spaces in terms of a constant times an enriched polynomial best approximation term.

Lemma 4.3. *Let u be any function in $H^1(\Omega)$. Then, for all u_π piecewise in $\tilde{\mathbb{P}}_p(K)$, there exists $u_I \in V_n$ such that*

$$|u - u_I|_{1,\mathcal{T}_n} \leq |u - u_\pi|_{1,\mathcal{T}_n}.$$

Proof. The proof follows along the same lines as that of [28, Proposition 3.8]. For the sake of completeness, we provide some details.

We define $u_I \in V_n$ by imposing the same degrees of freedom as u . More precisely, set

$$\begin{aligned} \int_K (u - u_I) q_{p-2} &= 0 \quad \forall q_{p-2} \in \mathbb{P}_{p-2}(K), \quad \forall K \in \mathcal{T}_n, \\ \int_e (u - u_I) \tilde{q}_{p-1}^e &= 0 \quad \forall \tilde{q}_{p-1}^e \in \tilde{\mathbb{P}}_{p-1}(e), \quad \forall e \in \mathcal{E}_n. \end{aligned} \quad (40)$$

Recall from the definition of the local virtual element spaces in (20) that, for all $e \in \mathcal{E}_n$ and $K \in \mathcal{T}_n$,

$$\mathbf{n}_K \cdot \nabla(u_I) \in \tilde{\mathbb{P}}_{p-1}(e), \quad \Delta u_I \in \mathbb{P}_{p-2}(K). \quad (41)$$

We deduce

$$\begin{aligned} |u - u_I|_{1,K}^2 &= \int_K \nabla(u - u_I) \cdot \nabla(u - u_I) \\ &= \int_K -\Delta(u - u_I)(u - u_I) + \int_{\partial K} \mathbf{n}_K \cdot \nabla(u - u_I)(u - u_I) \\ &\stackrel{(40),(41)}{=} \int_K -\Delta(u - u_\pi)(u - u_I) + \int_{\partial K} \mathbf{n}_K \cdot \nabla(u - u_\pi)(u - u_I) \\ &= \int_K \nabla(u - u_I) \cdot \nabla(u - u_\pi) \leq |u - u_\pi|_{1,K} |u - u_I|_{1,K}. \end{aligned}$$

The assertion follows dividing both sides by $|u - u_I|_{1,K}$ and summing over all the elements. \square

As a consequence, we have the following best interpolation result in nonconforming enriched virtual element spaces.

Proposition 4.4. *Let u be the solution to problem (11), u_0 be as in (10), and the assumptions (A0)-(A2) be valid. Then, there exists $u_I \in V_n$ such that*

$$|u - u_I|_{1,\mathcal{T}_n} \leq ch^p \left\{ \left(\sum_{K \in \mathcal{T}_n^1} |u_0|_{p+1,K}^2 \right)^{\frac{1}{2}} + \left(\sum_{K \in \mathcal{T}_n^2 \cup \mathcal{T}_n^3} |u|_{p+1,K}^2 \right)^{\frac{1}{2}} \right\},$$

where c is exactly the same constant appearing in the bound of Lemma 4.2.

Proof. Combine Lemmata 4.2 and 4.3. \square

4.4 Bound on the variational crime due to the right-hand side

Here, we show an upper bound on

$$\sup_{v_n \in V_n} \frac{\langle f, v_n \rangle - (f, v_n)_{0,\Omega}}{|v_n|_{1,\mathcal{T}_n}},$$

i.e., on the term representing the variational crime perpetrated in the discretization of the right-hand side in (1).

Lemma 4.5. *Given $p \in \mathbb{N}$, let $f \in H^{p-1}(\Omega)$. Under the assumptions (A0)-(A2), the following bound is valid:*

$$\sup_{v_n \in V_n} \frac{\langle f, v_n \rangle - (f, v_n)_{0,\Omega}}{|v_n|_{1,\mathcal{T}_n}} \leq ch^p \|f\|_{p-1,\Omega},$$

where c is a positive constant depending on p and on γ , being γ introduced in (A0)-(A2).

Proof. The proof is exactly the same as in the standard VE conforming setting: No special functions are used in the approximation of the right-hand side. See [10, Section 4.7] for more details. \square

4.5 Bound on the variational crime due to the nonconformity

Here, we prove an upper bound on the term

$$\sup_{v_n \in V_n} \frac{\mathcal{N}_n(u, v_n)}{|v_n|_{1,\mathcal{T}_n}},$$

i.e., the term representing the variational crime perpetrated when imposing the nonconformity of trial and test spaces.

Lemma 4.6. *Let u be the solution to problem (11), u_0 be as in (10), \mathcal{N}_n be defined in (35), and the assumptions (A0)-(A2) be valid. Then, we have*

$$\frac{\mathcal{N}_n(u, v_n)}{|v_n|_{1,\mathcal{T}_n}} \leq ch^p \left\{ \left(\sum_{K \in \mathcal{T}_n^1} |u_0|_{p,K}^2 \right)^{\frac{1}{2}} + \left(\sum_{K \in \mathcal{T}_n^2 \cup \mathcal{T}_n^3} |u|_{p,K}^2 \right)^{\frac{1}{2}} \right\},$$

where c is a positive constant depending on p and on γ , being γ introduced in (A0)-(A2).

Proof. We prove the bound edge by edge. Without loss of generality, we assume that $e \in \mathcal{E}_n^I$: The case $e \in \mathcal{E}_n^B$ can be treated analogously. Moreover, we assume that $e \in \mathcal{E}_n^1$: The case $e \in \mathcal{E}_n^2$ follows as in [4, Lemma 4.1].

Let K^+ and K^- be the two elements sharing the edge e . We write

$$\int_e \nabla u \cdot \llbracket v_n \rrbracket_e = \int_e \mathbf{n}_e \cdot \nabla u (v_n|_{K^+} - v_n|_{K^-}).$$

Denote the $L^2(e)$ projector onto constant functions on e by $\Pi_0^{0,e}$. The definition of the nonconforming enriched virtual element space in (29) and the properties of orthogonal projectors entail

$$\begin{aligned} \int_e \nabla u \cdot \llbracket v_n \rrbracket_e &= \int_e (\mathbf{n}_e \cdot \nabla u - \tilde{\Pi}_{p-1}^{0,e}(\mathbf{n}_e \cdot \nabla u))(v_n|_{K^+} - v_n|_{K^-} - \Pi_0^{0,e}(v_n|_{K^+} - v_n|_{K^-})) \\ &\leq \|\mathbf{n}_e \cdot \nabla u - \tilde{\Pi}_{p-1}^{0,e}(\mathbf{n}_e \cdot \nabla u)\|_{0,e} \|v_n|_{K^+} - v_n|_{K^-} - \Pi_0^{0,e}(v_n|_{K^+} - v_n|_{K^-})\|_{0,e}. \end{aligned} \quad (42)$$

We estimate the two terms on the right-hand side of (42) separately. We begin with the first one: For all $q_{p-1} \in \mathbb{P}_{p-1}(K)$,

$$\begin{aligned} &\|\mathbf{n}_e \cdot \nabla u - \tilde{\Pi}_{p-1}^{0,e} \mathbf{n}_e \cdot \nabla u_n\|_{0,e} \\ &\leq \|\mathbf{n}_e \cdot \nabla u_0 - \tilde{\Pi}_{p-1}^{0,e}(\mathbf{n}_e \cdot \nabla u_0)\|_{0,e} + \|\mathbf{n}_e \cdot \nabla \mathcal{S}_\mathbf{A} - \tilde{\Pi}_{p-1}^{0,e}(\mathbf{n}_e \cdot \nabla \mathcal{S}_\mathbf{A} \cdot \mathbf{n})\|_{0,e} \\ &\leq \|\mathbf{n}_e \cdot \nabla u_0 - \mathbf{n}_e \cdot \nabla q_{p-1}\|_{0,e} \leq \|\nabla u_0 - \nabla q_{p-1}\|_{0,e}. \end{aligned}$$

Apply the trace inequality and the Poincaré inequality, in addition to assumption **(A2)**, to get

$$\|\mathbf{n}_e \cdot \nabla u - \tilde{\Pi}_{p-1}^{0,e}(\mathbf{n}_e \cdot \nabla u)\|_{0,e} \lesssim h_K^{\frac{1}{2}} |\nabla u_0 - \nabla q_{p-1}|_{1,K}.$$

Use standard polynomial approximation theory [17] and assumption **(A1)** to arrive at

$$\|\mathbf{n}_e \cdot \nabla u - \tilde{\Pi}_{p-1}^{0,e}(\mathbf{n}_e \cdot \nabla u)\|_{0,e} \lesssim h_K^{p-\frac{1}{2}} |u_0|_{p,K}$$

Focus now on the second term on the right-hand side of (42). As proven in [4, Lemma 4.1],

$$\|v_n|_{K^+} - v_n|_{K^-} - \Pi_0^{0,e}(v_n|_{K^+} - v_n|_{K^-})\|_{0,e} \lesssim h^{\frac{1}{2}} |v_n|_{1,K^+ \cup K^-}.$$

The assertion follows summing over all the edges. \square

4.6 Stabilizations

Here, we exhibit explicit choices of the stabilization S^K introduced in (30) and discuss their properties. More precisely, we exhibit a theoretical stabilization, for which we are able to prove the bounds in (30) explicitly, and we introduce a practical stabilization, which we will employ in the numerical experiments in Section 5.

The theoretical stabilization. For every $K \in \mathcal{T}_n$, define

$$S_T^K(u_n, v_n) = h_K^{-2} (\Pi_{p-2}^{0,K} u_n, \Pi_{p-2}^{0,K} v_n) + h_K^{-1} (\tilde{\Pi}_{p-1}^{0,e} u_n, \tilde{\Pi}_{p-1}^{0,e} v_n)_{0,\partial K} \quad \forall u_n, v_n \in V_n(K). \quad (43)$$

Recall that the projector $\Pi_{p-2}^{0,K}$ is defined in (27), whereas the projector $\tilde{\Pi}_{p-1}^{0,e}$ is defined in (26).

Proposition 4.7. *Let the assumptions **(A0)**-**(A2)** be valid. Then, the stabilization defined in (43) satisfies (30).*

Proof. First, we show the lower bound. For every $v_n \in \ker(\tilde{\Pi}_p^{\nabla,K})$, using the definition of the local enriched spaces $V_n(K)$, we write

$$|v_n|_{1,K}^2 = \int_K \nabla v_n \cdot \nabla v_n = \int_K -\Delta v_n \Pi_{p-2}^{0,K} v_n + \int_{\partial K} \mathbf{n}_K \cdot \nabla v_n \tilde{\Pi}_{p-1}^{0,e} v_n.$$

Use the Cauchy-Schwarz inequality to get

$$|v_n|_{1,K} \leq \|\Delta v_n\|_{0,K} \|\Pi_{p-2}^{0,K} v_n\|_{0,K} + \|\mathbf{n}_K \cdot \nabla v_n\|_{0,\partial K} \|\tilde{\Pi}_{p-1}^{0,e} v_n\|_{0,\partial K}. \quad (44)$$

Equivalence of norms in finite dimensional spaces and a scaling argument give

$$\|\mathbf{n}_e \cdot \nabla v_n\|_{0,\partial K} \lesssim h_K^{-\frac{1}{2}} \|\mathbf{n}_e \cdot \nabla v_n\|_{-\frac{1}{2},\partial K}.$$

The following inverse inequality is valid; see [19, Lemma 10] and [12, Theorem 2]:

$$\|\Delta v_n\|_{0,K} \lesssim h_K^{-1} |v_n|_{1,K}. \quad (45)$$

The hidden constant depends on the degree of accuracy p and on the shape of the element K .

The Neumann trace inequality is valid as well; see, e.g., [34, Theorem A.33]:

$$\|\mathbf{n}_K \cdot \nabla v_n\|_{-\frac{1}{2},\partial K} \lesssim |v_n|_{1,K} + h_K \|\Delta v_n\|_{0,K} \stackrel{(45)}{\lesssim} |v_n|_{1,K}. \quad (46)$$

Collecting (44), (45), and (46) leads to

$$|v_n|_{1,K} \lesssim h_K^{-1} \|\Pi_{p-2}^{0,K} v_n\|_{0,K} + h_K^{-\frac{1}{2}} \|\tilde{\Pi}_{p-1}^{0,e} v_n\|_{0,\partial K},$$

which is the lower bound.

Next, we show the upper bound. We estimate from above the two terms on the right-hand side of the following identity:

$$S_T^K(v_n, v_n) = h_K^{-2} \|\Pi_{p-2}^{0,K} v_n\|_{0,K}^2 + h_K^{-1} \|\tilde{\Pi}_{p-1}^{0,e} v_n\|_{0,\partial K}^2.$$

As for the first term, we use the stability of orthogonal projections and the Poincaré inequality:

$$h_K^{-2} \|\Pi_{p-2}^{0,K} v_n\|_{0,K}^2 \lesssim |v_n|_{1,K}^2.$$

As for the second term, use the stability of orthogonal projections, the trace inequality, the Poincaré inequality, and the assumption **(A2)**:

$$h_K^{-1} \|\tilde{\Pi}_{p-1}^{0,e} v_n\|_{0,\partial K}^2 \lesssim |v_n|_{1,K}^2.$$

This concludes the proof. \square

The practical stabilization. The stabilization S_T^K introduced in (43) is computable in terms of the degrees of freedom (21) and (22). Notwithstanding, it requires a certain amount of work to implement.

Thence, we suggest to use the following practical stabilization, which is defined on the local canonical basis (23) as follows: For all $K \in \mathcal{T}_n$,

$$S_P^K(\varphi_i, \varphi_j) = \max(1, a^K (\tilde{\Pi}_p^{\nabla,K} \varphi_i, \tilde{\Pi}_p^{\nabla,K} \varphi_j)) \quad \forall i, j = 1, \dots, \dim(V_n(K)). \quad (47)$$

Originally, such stabilization was introduced for the standard 3D VEM in [13], and its performance was analysed in the 2D case in [27]. To the best of our knowledge, such stabilization is amongst the most robust from the numerical standpoint in the literature. Roughly speaking, this stabilization keeps trace somehow of the true energy of the canonical basis functions.

In Section 5 below, we perform the numerical experiments using the stabilization S_P^K in (47).

4.7 Convergence of the method

In this section, we collect all the a priori bounds hitherto proven, and we show a convergence result for the h -version of the method (33).

Theorem 4.8. *Let u and u_n be the solutions to (11) and (33), respectively, u_0 be as in (10), and the assumptions **(A0)**-**(A2)** be valid. Then, we have the following a priori h -convergence result:*

$$|u - u_n|_{1,\mathcal{T}_n} \leq ch^p \left\{ \left(\sum_{K \in \mathcal{T}_n^1} \|u_0\|_{p+1,K}^2 + \sum_{K \in \mathcal{T}_n^2 \cup \mathcal{T}_n^3} \|u\|_{p+1,K}^2 \right)^{\frac{1}{2}} + \|f\|_{p-1,\Omega} \right\}, \quad (48)$$

where c is a positive constant independent of h and u , but which possibly depends on the degree of accuracy p , the parameter γ introduced in **(A0)**-**(A2)**, and the singular function \mathcal{S}_A^K .

Proof. Combine Theorem 4.1, Lemma 4.2, Proposition 4.4, Lemma 4.5, Lemma 4.6, and Proposition 4.7. \square

Remark 2. Recall that the elements K in the first layer \mathcal{T}_n^1 are such that

- (i) either K abuts or contains **A**;
- (ii) or K is not too far apart from **A**.

In particular, $\text{dist}(\mathbf{A}, \mathbf{x}_K) \leq \tilde{\gamma} \text{diam}(\Omega)$, where $\gamma \in (0, 1)$ is a given parameter. The reason why \mathcal{T}_n^1 does not consist of elements abutting **A** only is that a uniform h -refinement implies

$$|\Omega| - \sum_{K \in \mathcal{T}_n^2 \cup \mathcal{T}_n^3} |K| \rightarrow 0 \quad \text{as } h \rightarrow 0.$$

This has to be avoided, for otherwise the second term on the right-hand side of (48) would blow up. \blacksquare

4.8 Generalizations

We devote this section to discuss some generalizations of the method (33).

Multiple singularities. The first generalization is when the expansion (10) is substituted by the general case (9). We discuss two generalization.

The first one is when we associate more singular functions at one singular vertex/tip. The extension from the unique singular function is rather straightforward: It suffices to add more singular functions to the local spaces $V_n(K)$, for all $K \in \mathcal{T}_n$ close to \mathbf{A} .

The second generalization is when there are more than one singular vertex/tip. In this case, we define the first layer \mathcal{T}_n^1 as the set of all elements close to one or more singular vertices-tips. Thus, the local spaces are enriched with special functions having singularities at different points.

The 3D case. In 3D, the singularities arising from the geometry of the domain are different from those in the 2D case. Nonetheless, all of them consist of harmonic functions; see, e.g., [33] and the references therein. In particular, vertex and edge singularities have to be dealt with.

The advantage of employing nonconforming virtual element spaces over conforming ones is that the definition of the local spaces is the same as in the two dimensional case: Given \mathcal{T}_n a polyhedral decomposition of the physical domain, for all $K \in \mathcal{T}_n$, we set

$$V_n(K) = \left\{ v_n \in H^1(K) \mid \Delta v_n \in \mathbb{P}_{p-2}(K), \mathbf{n} \cdot \nabla v_n|_F \in \tilde{\mathbb{P}}_{p-1}(F) \ \forall F \text{ face of } K \right\}.$$

Here, $\tilde{\mathbb{P}}_{p-1}(K)$ denotes the space of the polynomials of degree at most $p-1$ over a face F , possibly enriched of the normal derivative of the singular functions we add to the local spaces.

The construction of the method, as well as its analysis, follows exactly along the same lines as those of the two dimensional case.

Other differential operators. It is possible to generalize our setting to PDEs with more general elliptic operators.

Let \mathcal{L} be an elliptic differential operator of the second order, f a smooth datum, and γ_1 a trace operator. Consider the following problem: Find u such that

$$\begin{cases} \mathcal{L}u = f & \text{in } \Omega \\ \gamma_1 u = 0 & \text{on } \partial\Omega. \end{cases} \quad (49)$$

If \mathcal{L} is an elliptic operator, then the solution to problem (49) presents some singularities due to the geometry of the domain, and more specifically at corners, edges, tips of cracks, etc. In case the singular behaviour is known explicitly, the solution can be decomposed as in (9) into a combination of a smooth and a singular part.

For simplicity, consider the case of a unique singular function \mathcal{S} . Such \mathcal{S} belongs to the kernel of the operator \mathcal{L} , i.e., $\mathcal{L}(\mathcal{S}) = 0$. Thus, on every element $K \in \mathcal{T}_n$ sufficiently close to the singular corner, tip, edge etc., we define the local space

$$V_n(K) := \{ v_n \in H \mid \mathcal{L}v_n \in [\mathbb{P}_{p_1}(K)]^{\ell_1}, \gamma_2(v_n)|_e \in [\mathbb{P}_{p_2}(e)]^{\ell_2} \oplus \gamma_2(\mathcal{S}) \ \forall e \in \mathcal{E}^K \} \quad \ell_1, \ell_2 \in \mathbb{N}.$$

Here, H and $\gamma_2(\cdot)$ denote a suitable Sobolev space and a suitable trace operator, respectively.

We postpone the generalization presented in this section to future works.

5 Numerical results

In this section, we present some numerical experiments, which allow us to validate the theoretical results discussed in Section 4.

Errors. In order to measure the convergence of the method, we cannot use the exact relative error

$$\frac{|u - u_n|_{1, \mathcal{T}_n}}{|u|_{1, \Omega}}. \quad (50)$$

In fact, the discrete solution u_n is not known in closed-form, but only through its degrees of freedom. Therefore, we measure the decay of the following *computable* relative error: Given $\tilde{\Pi}_p^{\nabla, K}$ defined piecewise as $\tilde{\Pi}_p^{\nabla, K}$ over \mathcal{T}_n ,

$$\frac{|u - \tilde{\Pi}_p^{\nabla, K} u_n|_{1, \mathcal{T}_n}}{|u|_{1, \Omega}}. \quad (51)$$

The two errors (50) and (51) have the same convergence rate in terms of the mesh size h . In order to see this, on the one hand, we use the stability of the H^1 projection to get

$$|u - \tilde{\Pi}_p^{\nabla} u_n|_{1, \mathcal{T}_n} \leq |u - \tilde{\Pi}_p^{\nabla} u|_{1, \mathcal{T}_n} + |\tilde{\Pi}_p^{\nabla} u - \tilde{\Pi}_p^{\nabla} u_n|_{1, \mathcal{T}_n} \leq |u - \tilde{\Pi}_p^{\nabla} u|_{1, \mathcal{T}_n} + |u - u_n|_{1, \mathcal{T}_n}.$$

The convergence of the first term on the right-hand side is provided by Lemma 4.2.

On the other hand, we use Theorem 4.1 and Proposition 4.4 to get

$$\begin{aligned} |u - u_n|_{1, \mathcal{T}_n} &\lesssim \max_{K \in \mathcal{T}_n} \alpha_*^{-1}(K) \left\{ \sup_{v_n \in V_n} \frac{\langle f, v_n \rangle_n - (f, v_n)_{0, \Omega}}{|v_n|_{1, \mathcal{T}_n}} + \sup_{v_n \in V_n} \frac{\mathcal{N}_n(u, v_n)}{|v_n|_{1, \mathcal{T}_n}} \right. \\ &\quad \left. + \left(1 + \max_{K \in \mathcal{T}_n} \alpha^*(K) \right) |u - \tilde{\Pi}_p^{\nabla} u_n|_{1, \mathcal{T}_n} \right\}. \end{aligned}$$

The convergence of the first two terms on the right-hand side is provided by Lemmata 4.5 and 4.6.

Enriched polynomial basis functions. We introduce the basis functions for the standard and enriched bulk and edge polynomial spaces. Consider the natural bijection between \mathbb{N} and $\mathbb{N}_0 \times \mathbb{N}_0$ given by

$$1 \leftrightarrow (0, 0), \quad 2 \leftrightarrow (1, 0), \quad 3 \leftrightarrow (0, 1), \quad 4 \leftrightarrow (2, 0), \quad 5 \leftrightarrow (1, 1), \quad 6 \leftrightarrow (0, 2) \quad \dots \quad (52)$$

Henceforth, given a positive integer scalar α , we denote the relative vector through the above bijection by $\alpha = (\alpha_1, \alpha_2)$.

Let $\mathbf{x}_K = (x_K, y_K)$ be the centroid of K , for all $K \in \mathcal{T}_n$. For all $K \in \mathcal{T}_n$, as for the space $\mathbb{P}_p(K)$, we consider the basis elements defined as scaled and centred monomials

$$m_\alpha^K(\mathbf{x}) := \left(\frac{x - x_K}{h_K} \right)^{\alpha_1} \left(\frac{y - y_K}{h_K} \right)^{\alpha_2} \quad \forall \alpha = 1, \dots, \dim(\mathbb{P}_p(K)). \quad (53)$$

As for the bulk enriched polynomial space $\tilde{\mathbb{P}}_p(K)$, we consider the monomials in (53) *plus* the function $\mathcal{S}_{\mathbf{A}}^K$ defined in (17) as basis elements.

Denote the Legendre polynomial of degree $\alpha \in \mathbb{N}$ on $[-1, 1]$ by $\mathbb{L}_\alpha(x)$. Given $e \in \mathcal{E}_n$, denote the linear transformation mapping the interval $[-1, 1]$ to the edge e by Φ_e . For all $e \in \mathcal{E}_n$, as for the space $\mathbb{P}_{p-1}(e)$, we consider the basis elements defined as scaled and centred Legendre polynomials

$$\mathbb{L}_\alpha^e(\mathbf{x}) := \mathbb{L}_\alpha(\Phi_e^{-1}(\mathbf{x})) \quad \forall \alpha = 1, \dots, \dim(\mathbb{P}_{p-1}(e)). \quad (54)$$

As for the enriched polynomial space $\tilde{\mathbb{P}}_{p-1}(e)$, we consider the Legendre polynomials in (54) *plus* the function $\mathbf{n}_e \cdot \nabla \mathcal{S}_{\mathbf{A}|e}^e$, where $\mathcal{S}_{\mathbf{A}}^e$ is defined in (18), as basis elements.

For future convenience, the basis elements for the bulk enriched polynomial spaces are denoted by

$$\tilde{m}_\alpha^K \quad \forall \alpha = 1, \dots, \dim(\tilde{\mathbb{P}}_p(K)),$$

whereas for the edge enriched polynomial spaces

$$\tilde{m}_\alpha^e \quad \forall \alpha = 1, \dots, \dim(\tilde{\mathbb{P}}_{p-1}(e)).$$

Stabilization. We employ the stabilization defined in (47).

Remark 3. The nonconforming setting allows for an effective improvement of the condition number of the final system. In order to get such improvement, we suggest to orthogonalize the basis functions of the edge and bulk enriched polynomial basis functions. This is very much in the spirit of [27]. We avoid further discussions on this issue, to keep the matter as simple as possible.

Next, we present the test cases we will analyse numerically.

Test case 1. The first test case is defined on the L-shaped domain

$$\Omega_1 = (-1, 1)^2 \setminus [0, 1) \times (-1, 0]. \quad (55)$$

Let (r, θ) be the polar coordinates at the re-entrant corner $(0, 0)$. We are interested in the approximation of the exact solution

$$u_1(x, y) = u_1(r, \theta) = \sin(\pi x) \sin(\pi y) + r^{\frac{2}{3}} \sin\left(\frac{2}{3}\theta\right). \quad (56)$$

The primal formulation of the problem we are interested in is such that we have: zero Dirichlet boundary conditions on the edges generating the re-entrant corner; suitable Dirichlet boundary conditions on all the other edges a right-hand computed accordingly to (56). The right-hand side is smooth since the singular function is harmonic.

Test case 2. The second test case is defined on the slit square domain

$$\Omega_2 := (-1, 1)^2 \setminus \{(x, y) \in \mathbb{R}^2 \mid x \geq 0\}.$$

We consider a solution, which is singular only at the tip of the slit $(0, 0)$. Let (r, θ) be the polar coordinates at such tip, with $\theta \in [0\pi, 2\pi)$. We are interested in the approximation of the exact solution

$$u_2(r, \theta) = r^{\frac{1}{2}} \sin\left(\frac{1}{2}\theta\right). \quad (57)$$

The primal formulation of the problem we are interested in is such that we have: suitable Dirichlet boundary conditions on all the edges; zero right-hand side, since u_3 is harmonic.

Meshes. In the forthcoming numerical experiments, we employ sequences of uniform Cartesian meshes; see Figure 5 for examples of such meshes for the two test cases. As for the test case 2, we highlight the slit in colour: the couples of adjacent squares do *not* share the same edge.

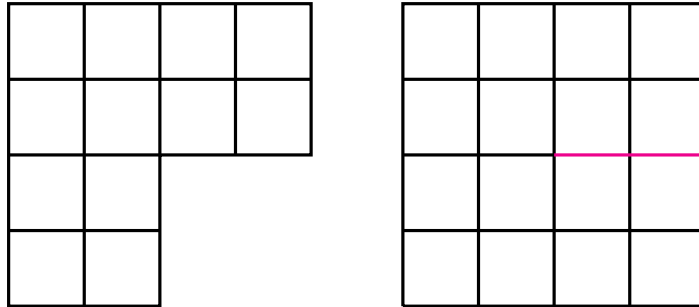


Figure 5: Meshes that we employ in the numerical experiments. *Left panel:* test case 1. *Right panel:* test case 2.

We depict the first mesh of the sequence of meshes for the test case 2 in Figure 6: It consists of a single heptagonal element with two edges having endpoints sharing coordinates. Thus, we show that the virtual element method works and is robust also on degenerate polygons.

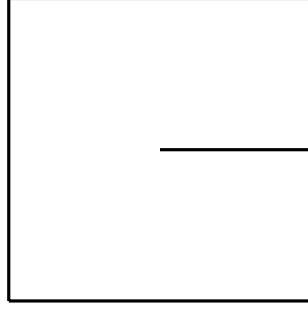


Figure 6: First mesh of the sequence of meshes employed for the test case 2. It consists of a single heptagonal element with two edges having endpoints sharing coordinates.

Layers. We consider different distributions of the layers; see Section 3.2. We test the method assuming that all the elements of the mesh belong to the first layer defined in (15), i.e., we enrich all the local spaces. Furthermore, we consider the partially enriched scheme, i.e., we enrich only the elements, which lie in a neighbourhood of the singular point **A**. In Figure 7, we depict the two different layerisations for the same Cartesian mesh for the test case 1. We pick $\tilde{\gamma} = 1/10$ in (15). A similar layerisation is valid for the test case 2 and is therefore not shown. Further, we will compare the new enriched method with the standard one [4]. In this case, all the elements belong to the third layer defined in (16).

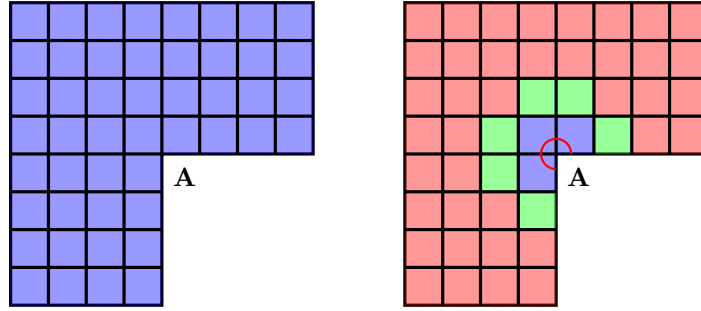


Figure 7: Two different layerisations for the same Cartesian mesh on the L-shaped domain Ω_1 in (55). *Left panel:* all the elements belong to the enriched layer \mathcal{T}_n^1 . *Right panel:* there are three layers; we pick $\tilde{\gamma} = 1/10$ in (15). We depict: in blue, the elements in the first element layer \mathcal{T}_n^1 ; in green, the elements in the second element layer \mathcal{T}_n^2 ; in red, the elements in the third layer \mathcal{T}_n^3 .

5.1 Numerical experiments on the L-shaped domain

In this section, we present several numerical experiments for the test case 1, with exact solution u_1 defined in (56), using the fully enriched, the partially enriched, and the standard [4] schemes. Notably, we are interested in the performance of the h - and the p -versions of the method, which are the topic of Sections 5.1.1 and 5.1.2, respectively. We investigate two additional computational aspects in Sections 5.1.3 and 5.1.4. First, on a single mesh, we tune the parameter $\tilde{\gamma}$ in (15) in order to optimize the error of the method; next, we provide a heuristic motivation as for why the fully enriched scheme turns out to be less stable than the partially enriched one.

5.1.1 The h -version

In Figure 8, we present numerical results for the h -version of the method. We consider the exact solution u_1 in (56) and the degrees of accuracy $p = 1, 2$, and 3. We use sequences of Cartesian meshes as those in Figure 5, and compare the performance of the fully enriched (left) and partially enriched methods (right). Further, we plot the error of the standard nonconforming VEM of [4]; see Figure 8 (bottom).

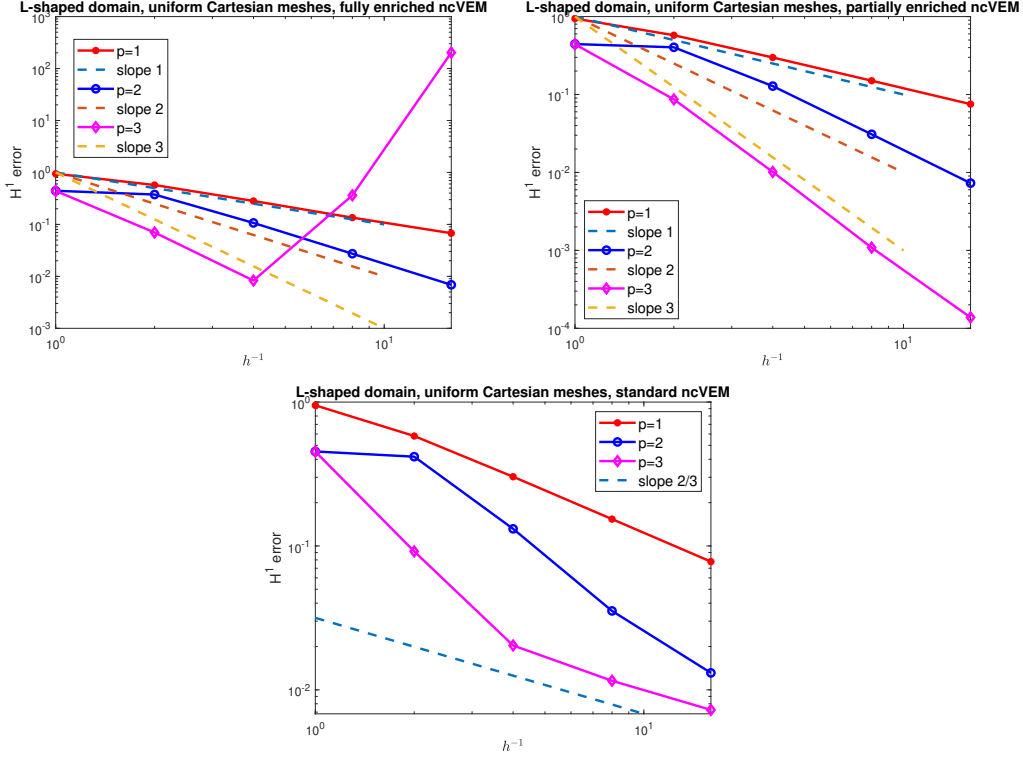


Figure 8: h -version of various versions of the method in order to approximate the exact solution u_1 in (56). The polynomial degree of accuracy of the method is $p = 1, 2$, and 3 . We employ sequences of uniform Cartesian meshes as those in Figure 5 (left). *Left panel:* fully enriched method. *Right panel:* partially enriched method ($\tilde{\gamma} = 1/10$). *Bottom panel:* standard method.

In Figure 8 (left) and (right), we observe an optimal rate of convergence. In particular, for all the three degrees of accuracy p , the two enriched method converge with order p . On the other hand, see Figure 8 (bottom), the standard method converges suboptimally, which we can expect from the analysis of [4].

The fully enriched scheme suffers from a loss a convergence for fine meshes. We investigate the reasons of this phenomenon in Section 5.1.4 below.

5.1.2 The p -version

In Figure 9, we investigate the behaviour of the p -version of the fully and partially enriched ($\tilde{\gamma} = 1/10$) versions of the method. Further, we plot the decay of the error employing the standard nonconforming VEM of [4]. We consider the exact solution u_1 in (56) and we fix a uniform Cartesian mesh consisting of 48 elements. What we could expect combining the standard theory for the p -version of Galerkin methods, see, e.g., [8], and the analysis developed in this paper, is that the enriched method converges exponentially in terms of p . On the other hand, we expect an algebraic rate of convergence for the standard method.

From Figure 9, we observe several facts. The standard version of the nonconforming VEM converges algebraically, whereas the error computed with the fully enriched method blows up. This is due to the ill-conditioning of the final system; see Section 5.1.4 below.

More surprisingly, the partially enriched method presents an exponential pre-asymptotic behaviour, up to $p = 3$, but then the convergence turns to be algebraic. This is due again to the ill-conditioning. When computing the error (51), round-off errors prevent us to have the correct coefficient in the expansion of $\tilde{\Pi}_p^{\nabla, K}$ so that we are not able to eliminate the singularity in the solution.

In future, we will investigate techniques to reduce such ill-conditioning and recover exponential convergence for the p -version. As a positive note, we observe that the p -version of the partially

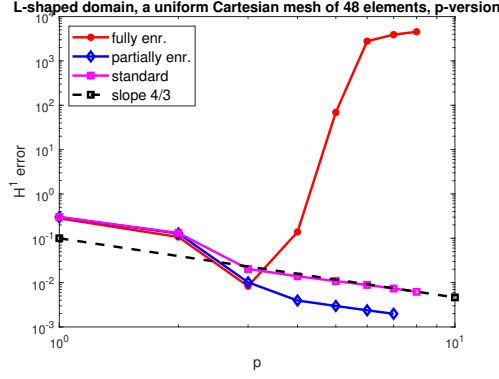


Figure 9: p -version of various versions of the method in order to approximate the exact solution u_1 in (56). We take a uniform Cartesian mesh consisting of 48 elements and employ the fully enriched, the partially enriched ($\tilde{\gamma} = 1/10$), and the standard methods.

enriched method performs one order of magnitude better than the standard one.

5.1.3 On the parameter $\tilde{\gamma}$ in (15)

In this section, we investigate how the choice of the parameter $\tilde{\gamma}$ appearing in (15) influences the performance of the method. To this aim, consider the exact solution u_1 in (56), fix a uniform Cartesian mesh with 192 elements, consider 14 equispaced values of $\tilde{\gamma}$ in $(0.1, 1.4)$, and depict the error of the method for each choice of the parameter in Figure 10.

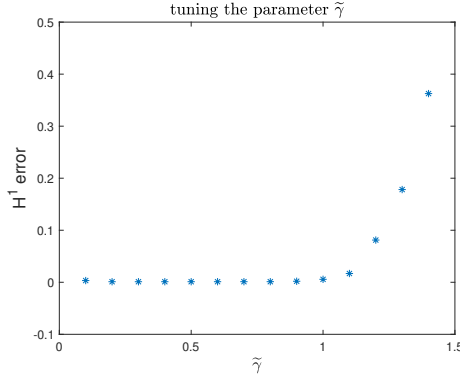


Figure 10: Performance of the partially enriched method picking different $\tilde{\gamma}$ in (15). In particular, we pick 14 equispaced values of $\tilde{\gamma}$ in $(0.1, 1.4)$. The exact solution is u_1 in (56). We employ a uniform Cartesian mesh with 192 elements.

It turns out that the optimal choice of the parameter $\tilde{\gamma}$ lies in the range $\tilde{\gamma} \in (0.1, 1)$. For larger choices of the parameter, the error grows as the ill-conditioning of the system increases. Needless to say, the above analysis of the best parameter is valid for the current test case and ought to be performed for every exact solution.

5.1.4 Why is the fully enriched scheme less stable than the partially enriched one?

In Sections 5.1.1 and 5.1.3, we observed that the fully enriched scheme is less stable than the partially enriched one; see Figure 8. In this section, we give some heuristic motivations as for the reason why this happens.

The motivation behind the growth of the ill-conditioning for fine meshes is due to the behaviour of the singular enrichment function $\mathcal{S}_{\mathbf{A}}^K$. On the elements that are close to the singular vertex \mathbf{A} , $\mathcal{S}_{\mathbf{A}}^K$ differs from all the scaled monomials, which span the standard polynomial basis. On the other hand, on the elements that are far from \mathbf{A} , the singular function $\mathcal{S}_{\mathbf{A}}^K$ becomes close to a constant

function, especially for small elements. In a sense, the basis functions of the virtual element space become close to be linearly dependent, as keeping on refining the mesh.

In Figure 11, we depict the singular function $\mathcal{S}_{\mathbf{A}}^K$ with singular behaviour given by $\alpha = 2/3$ and a constant function along the radial component on two intervals of length 0.03. The first one (left) is close to \mathbf{A} , the second one (right) is slight far from it.

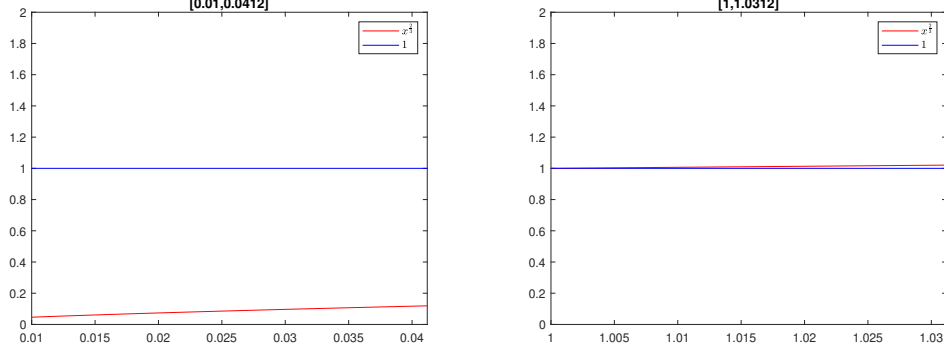


Figure 11: Behaviour of $\mathcal{S}_{\mathbf{A}}$ and a constant function along the radial component. *Left panel:* interval $[0.01, 0.04]$. *Right panel:* interval $[0.01, 0.04]$.

From Figure 11, it is apparent that the singular functions get extremely close to a constant function, thus leading to an ill-conditioned system. A possible remedy to this situation could be to use bulk and edgewise orthogonalizing techniques as those presented in [27].

5.2 Numerical experiments on the slit domain: the extended patch test

In this section, we verify that the method works also on the test case with exact solution u_2 in (57). We investigate the performance of the h -version of the method only, employing sequences of uniform Cartesian meshes as in Figure 5 (right).

The test case 1 can be regarded as an extended patch test: The exact solution is equal, up to constants, to the enrichment function $\mathcal{S}_{\mathbf{A}}^K$. Thence, if we consider the fully enriched version of the method then the error is zero up to machine precision, thanks to the enriched consistency of the discrete bilinear forms in (32). In Figure 12, we depict the decay of the error of the method for $p = 1, 2$, and 3. We consider the fully version of the method.

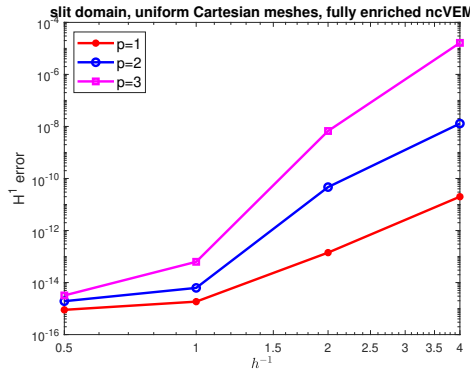


Figure 12: h -version of the fully enriched version of the method in order to approximate the exact solution u_2 in (57). The polynomial degree of accuracy of the method is $p = 1, 2$, and 3. We employ sequences of uniform Cartesian meshes as those in Figure 5 (right).

From Figure 12, we realize that the fully enriched method returns an error, which is zero up to machine precision as expected from the enriched consistency (32). The growth of the error for this enriched patch test is an excellent indicator for the growth of the ill-conditioning of the system. Finally, we have evidence that the VEM works also on very particular polygonal meshes, including

elements with internal cracks: The first element of the sequence of meshes is the heptagon with two overlapping edges depicted in Figure 6.

6 Conclusions

We introduced an enriched virtual element method for the approximation of solutions to the Laplace problem on polygonal domain. This has been done in the spirit of the extended Galerkin methods, but with a novel twist. The standard virtual element spaces are endowed with special singular functions arising from asymptotic singular expansions at the corners of the domain. We analysed the method and presented several numerical results, including the high-order version of the method, which validate the theoretical predictions. In the Appendix below, we discuss the implementation details. Importantly, both the theoretical and practical aspects are extensions of what is done in standard nonconforming virtual element methods.

In future works, we plan to investigate some generalizations of this approach:

- multiple singularities;
- the 3D version of the method;
- enriched virtual elements for more general elliptic operators;
- mitigate the ill-conditioning by means of orthogonalization techniques as those presented in [27].

A Implementation details

Here, we discuss the implementation details of the method. We employ the same notation as in [11]. As in standard nonconforming finite and virtual elements, the global stiffness matrix is obtained by assembling the local ones. Therefore, we show the computation of the local stiffness matrices only. We focus on the elements K in the first layer \mathcal{T}_n^1 only: The local stiffness matrices on the elements $K \in \mathcal{T}_n^3$ are computed as in [4], whereas it suffices to combine the tools employed for the other two layers on the elements $K \in \mathcal{T}_n^2$.

Recall that we are assuming (10), i.e., we enrich the approximation space with one singular function only. The implementation details are utterly similar in the case of multiple singularities.

Following [11], the local matrix on the element $K \in \mathcal{T}_n$ is given by

$$\mathbf{A}_n^K = \mathbf{\Pi}^{*T} \mathbf{G} \mathbf{\Pi}^* + (\mathbf{I} - \mathbf{\Pi})^T \mathbf{S} (\mathbf{I} - \mathbf{\Pi}). \quad (58)$$

We define the various matrices appearing in (58). We begin with

$$\mathbf{G}_{\alpha,\beta} = \begin{cases} (\nabla \tilde{m}_\beta, \nabla \tilde{m}_\alpha)_{0,K} & \forall \alpha, \beta = 2, \dots, \dim(\tilde{\mathbb{P}}_p(K)) \\ 0 & \text{otherwise.} \end{cases}$$

The matrix $\mathbf{\Pi}^*$ is the matrix representation of the expansion of the projector $\tilde{\Pi}_p^{\nabla,K}$ in terms of the basis functions of $\tilde{\mathbb{P}}_p(K)$:

$$\mathbf{\Pi}^* = \tilde{\mathbf{G}}^{-1} \mathbf{B},$$

where

$$\tilde{\mathbf{G}}_{\alpha,\beta} = \begin{cases} (\nabla \tilde{m}_\beta, \nabla \tilde{m}_\alpha)_{0,K} & \alpha, \beta = 2, \dots, \dim(\tilde{\mathbb{P}}_p(K)) \\ \frac{1}{|\partial K|} \int_{\partial K} \tilde{m}_\alpha & \text{otherwise,} \end{cases} \quad (59)$$

and

$$\mathbf{B}_{\alpha,i} = \begin{cases} (\nabla \varphi_i, \nabla \tilde{m}_\alpha) & \forall \alpha = 2, \dots, \dim(\tilde{\mathbb{P}}_p(K)), \forall i = 1, \dots, \dim(V_n(K)) \\ \frac{1}{|\partial K|} \int_{\partial K} \varphi_i & \text{otherwise.} \end{cases} \quad (60)$$

The matrix $\mathbf{\Pi}$ is the matrix representation of the expansion of the projector $\tilde{\Pi}_p^{\nabla, K}$ in terms of the basis functions of $V_n(K)$:

$$\mathbf{\Pi} = \mathbf{D}\mathbf{\Pi}^*,$$

where

$$\mathbf{D}_{i,\alpha} = \text{dof}_i(\tilde{m}_\alpha) \quad \forall i = 1, \dots, \dim(V_n(K)), \quad \forall \alpha = 1, \dots, \dim(\tilde{\mathbb{P}}_p(K)).$$

Finally, \mathbf{S} is the matrix representation of the stabilization, i.e.,

$$\mathbf{S}_{i,j} = S_P^K(\varphi_j, \varphi_i) \quad \forall i, j = 1, \dots, \dim(V_n(K)).$$

If we employ the stabilization introduced in (47), then the matrix \mathbf{S} is diagonal, with entries given by the maximum between 1 and the corresponding diagonal entries of the consistency matrix $\mathbf{\Pi}^{*T} \mathbf{G} \mathbf{\Pi}^*$.

We devote the remainder of this section to show how to compute the matrices \mathbf{G} , $\tilde{\mathbf{G}}$, \mathbf{B} , and \mathbf{D} . We fix the following notation:

$$\begin{aligned} n_p^K &= \dim(\mathbb{P}_p(K)), & n_{p-1}^e &= \dim(\mathbb{P}_{p-1}(e)), \\ \tilde{n}_p^K &= \dim(\tilde{\mathbb{P}}_p(K)), & \tilde{n}_{p-1}^e &= \dim(\tilde{\mathbb{P}}_{p-1}(e)), & \tilde{N}^K &= \dim(V_n(K)). \end{aligned}$$

Moreover, we set

$$\tilde{\mathbb{P}}_p(K) = \text{span}_{\alpha=1}^{\tilde{n}_p^K} \{\tilde{m}_\alpha^K\}, \quad \tilde{\mathbb{P}}_{p-1}(e) = \text{span}_{\alpha=1}^{\tilde{n}_{p-1}^e} \{\tilde{m}_\alpha^e\},$$

where the functions \tilde{m}_α^K and \tilde{m}_α^e are defined in Section 5.

The atrices \mathbf{G} and $\tilde{\mathbf{G}}$. It suffices to show how to compute the matrix $\tilde{\mathbf{G}}$ in (59). Define

$$\tilde{\mathbf{G}}^A \in \mathbb{R}^{1 \times \tilde{n}_p^K}, \quad \tilde{\mathbf{G}}^B \in \mathbb{R}^{(\tilde{n}_p^K - 1) \times \tilde{n}_p^K},$$

as follows. Begin with $\tilde{\mathbf{G}}^A$:

$$\tilde{\mathbf{G}}_{1,\beta}^A = \frac{1}{|\partial K|} \int_{\partial K} \tilde{m}_\beta^K \quad \forall \beta = 1, \dots, \tilde{n}_p^K.$$

As for $\tilde{\mathbf{G}}^B$, we set

$$\tilde{\mathbf{G}}_{\alpha,\beta}^B = \int_K \nabla \tilde{m}_\alpha^K \cdot \nabla \tilde{m}_\beta^K \quad \forall \alpha = 2, \dots, \tilde{n}_p^K, \quad \beta = 1, \dots, \tilde{n}_p^K.$$

Each entry of $\tilde{\mathbf{G}}^A$ and $\tilde{\mathbf{G}}^B$ can be approximated at any precision, employing a sufficiently accurate quadrature formula.

The matrix $\tilde{\mathbf{G}} \in \mathbb{R}^{\tilde{n}_p^K \times \tilde{n}_p^K}$ is given by

$$\begin{bmatrix} \tilde{\mathbf{G}}^A \\ \tilde{\mathbf{G}}^B \end{bmatrix}.$$

The matrix \mathbf{B} . Denote the number of edges and vertices of K by N^V and define

$$\begin{aligned} \mathbf{B}^A &\in \mathbb{R}^{1 \times N^V p}, & \mathbf{B}^B &\in \mathbb{R}^{1 \times N^V}, & \mathbf{B}^C &\in \mathbb{R}^{1 \times n_{p-2}^K}, \\ \mathbf{B}^D &\in \mathbb{R}^{(n_p^K - 1) \times N^V p}, & \mathbf{B}^E &\in \mathbb{R}^{(n_p^K - 1) \times N^V}, & \mathbf{B}^F &\in \mathbb{R}^{(n_p^K - 1) \times n_{p-2}^K}, \\ \mathbf{B}^G &\in \mathbb{R}^{1 \times N^V p}, & \mathbf{B}^H &\in \mathbb{R}^{1 \times N^V}, & \mathbf{B}^I &\in \mathbb{R}^{1 \times n_{p-2}^K}. \end{aligned}$$

The matrix $\mathbf{B} \in \mathbb{R}^{\tilde{n}_p^K \times \tilde{N}^K}$ is given by

$$\begin{bmatrix} \mathbf{B}^A & \mathbf{B}^B & \mathbf{B}^C \\ \mathbf{B}^D & \mathbf{B}^E & \mathbf{B}^F \\ \mathbf{B}^G & \mathbf{B}^H & \mathbf{B}^I \end{bmatrix}.$$

In the matrix \mathbf{B} , the first column represents the contributions due to the basis elements associated with the standard edge polynomials; the second with special boundary functions; the third with the standard bulk polynomials. On the other hand, the first row represents the zero average constraint; the second the contributions of the standard bulk polynomials; the third the contributions of the singular bulk function.

Owing to (60) and the definition of the edge degrees of freedom in (22), we set

$$\mathbf{B}_{1,i}^B = 0 \quad \forall i = 1, \dots, N^V, \quad \mathbf{B}_{1,i}^C = 0 \quad \forall i = 1, \dots, n_{p-2}^K.$$

Denote the j -th edge in the local ordering of K by $e(j)$. The vector \mathbf{B}^A has the entries equal to $\frac{|e(j)|}{|\partial K|}$ in the j p -th column, for $j = 1, \dots, N^V$. Otherwise, it has zero entries.

Next, observe that an integration by parts yields

$$(\nabla \tilde{m}_\alpha^K, \nabla \varphi_i)_{0,K} = -(\Delta \tilde{m}_\alpha^K, \varphi_i)_{0,K} + \sum_{e \in \mathcal{E}^K} (\mathbf{n}_K \cdot \nabla \tilde{m}_\alpha^K, \varphi_i)_{0,e}. \quad (61)$$

If φ_i is an edge basis function, then the first term on the right-hand side of (61) vanishes. For all $e \in \mathcal{E}^K$, if \tilde{m}_α^K is a standard monomial, then we expand $\mathbf{n}_K \cdot \nabla \tilde{m}_\alpha^K|_e$ into a linear combination of scaled Legendre polynomials defined in (54):

$$\mathbf{n}_K \cdot \nabla \tilde{m}_\alpha^K|_e = \sum_{\beta=0}^{p-1} \lambda_\beta \mathbb{L}_\beta^e. \quad (62)$$

We identify the coefficients λ_α in the expansion (62) as follows: Test (62) with any scaled Legendre polynomial of degree at most $p-1$ and use the orthogonality property

$$(\mathbb{L}_\alpha^e, \mathbb{L}_\beta^e)_{0,e} = \frac{h_e}{2\beta+1} \delta_{\alpha,\beta} \quad \forall \alpha, \beta = 0, \dots, p-1, \quad (63)$$

to get

$$\lambda_\beta = \frac{2\beta+1}{h_e} (\mathbf{n}_K \cdot \nabla \tilde{m}_\alpha^K, \mathbb{L}_\beta^e)_{0,e} \quad \forall \beta = 0, \dots, p-1.$$

The integral on the right-hand side is computable exactly. Thus, the expansion (62) becomes

$$\mathbf{n}_K \cdot \nabla \tilde{m}_\alpha^K|_e = \sum_{\beta=0}^{p-1} \frac{2\beta+1}{h_e} (\mathbf{n}_K \cdot \nabla \tilde{m}_\alpha^K, \mathbb{L}_\beta^e)_{0,e} \mathbb{L}_\beta^e.$$

Given $e(i)$ the edge where the edge basis function φ_i has a nonzero edge moment, we write

$$\begin{aligned} (\nabla \tilde{m}_\alpha^K, \nabla \varphi_i)_{0,K} &= (\mathbf{n}_K \cdot \nabla \tilde{m}_\alpha^K|_{e(i)}, \varphi_i)_{0,e(i)} \\ &= \sum_{\beta=0}^{p-1} \frac{2\beta+1}{h_{e(i)}} (\mathbf{n}_K \cdot \nabla \tilde{m}_\alpha^K|_{e(i)}, \mathbb{L}_\beta^{e(i)})_{0,e(i)} (\mathbb{L}_\beta^{e(i)}, \varphi_i)_{0,e(i)}. \end{aligned}$$

Let $j_{e(i)}$ denote the numbering of φ_i as a basis function on edge $e(i)$. Using the definition of the edge degrees of freedom (22), we set

$$\begin{aligned} \mathbf{B}_{\alpha,i}^D &= (2(j_{e(i)} - 1) + 1) (\mathbf{n}_K \cdot \nabla \tilde{m}_\alpha^K|_{e(i)}, \mathbb{L}_i^{e(i)})_{0,e(i)} \quad \forall \alpha = 2, \dots, n_p^K - 1, \quad \forall i = 1, \dots, pN^V, \\ \mathbf{B}_{\alpha,i}^E &= 0 \quad \forall \alpha = 2, \dots, n_p^K - 1, \quad \forall i = 1, \dots, N^V. \end{aligned}$$

Next, consider the case of φ_i being an edge basis function and \tilde{m}_α^K being the special function $\mathcal{S}_{\mathbf{A}}^K$ defined in (17). From (19) and (61), we deduce

$$(\nabla \tilde{m}_\alpha^K, \nabla \varphi_i)_{0,K} = (\mathbf{n}_K \cdot \nabla \mathcal{S}_{\mathbf{A}}^K, \varphi_i)_{0,e(i)} = \mathbf{n}_K \cdot \mathbf{n}_{e(i)} \left(\frac{h_{e(i)}}{h_K} \right)^\alpha (\mathbf{n}_{e(i)} \cdot \nabla \mathcal{S}_{\mathbf{A}}^{e(i)}, \varphi_i)_{0,e(i)}.$$

Using the definition of the edge degrees of freedom (22), we set

$$\mathbf{B}_{1,i}^G = 0 \quad \forall i = 1, \dots, N^V p, \quad \mathbf{B}_{1,i}^H = \mathbf{n}_K \cdot \mathbf{n}_{e(i)} \left(\frac{h_{e(i)}}{h_K} \right)^\alpha \quad \forall i = 1, \dots, N^V.$$

Finally, focus on the case given by φ_i being a bulk basis function. Firstly, assume that $\tilde{m}_\alpha^K = m_\alpha^K$ is a standard polynomial. Given (x_K, y_K) the centroid of K , the following splitting is valid:

$$\begin{aligned} \Delta m_\alpha^K &= \Delta \left(\left(\frac{x - x_K}{h_K} \right)^{\alpha_1} \left(\frac{y - y_K}{h_K} \right)^{\alpha_2} \right) \\ &= \frac{1}{h_K^2} \left(\alpha_1(\alpha_1 - 1) \left(\frac{x - x_K}{h_K} \right)^{\alpha_1 - 2} \left(\frac{y - y_K}{h_K} \right)^{\alpha_2} + \alpha_2(\alpha_2 - 1) \left(\frac{x - x_K}{h_K} \right)^{\alpha_1} \left(\frac{y - y_K}{h_K} \right)^{\alpha_2 - 2} \right). \end{aligned}$$

Let α be associated to (α_1, α_2) via the bijection (52). Whenever it makes sense, set $\tilde{\alpha}_1$ and $\tilde{\alpha}_2$ the natural numbers associated with $(\alpha_1 - 2, \alpha_2)$ and $(\alpha_1 - 2, \alpha_2)$, respectively, via the same bijection (52).

We have

$$\begin{aligned} (\nabla m_\alpha^K, \nabla \varphi_i)_{0,K} &= -(\Delta m_\alpha^K, \varphi_i)_{0,K} \\ &= \begin{cases} 0 & \text{if } \alpha = 1, 2, 3 \\ -\frac{|K|}{h_K^2} \left((\alpha_1 - 1)\alpha_1 \frac{1}{|K|} (m_{\alpha_1}^K, \varphi_i)_{0,K} + (\alpha_2 - 1)\alpha_2 \frac{1}{|K|} (m_{\alpha_2}^K, \varphi_i)_{0,K} \right) & \text{otherwise.} \end{cases} \end{aligned}$$

In other words, we get

$$\begin{aligned} \mathbf{B}_{\alpha,i}^F &= \begin{cases} 0 & \text{if } \alpha = 1, 2, 3, \forall i = 2, \dots, n_{p-2}^K \\ -\frac{|K|}{h_K^2} ((\alpha_1 - 1)\alpha_1 \delta_{\tilde{\alpha}_1,i} + (\alpha_2 - 1)\alpha_2 \delta_{\tilde{\alpha}_2,i}) & \forall \alpha = 4, \dots, n_p^K, \forall i = 1, \dots, n_{p-2}^K, \end{cases} \\ \mathbf{B}_{1,i}^I &= 0 \quad \forall i = 1, \dots, n_{p-2}^K. \end{aligned}$$

The matrix \mathbf{D} . We introduce

$$\mathbf{D}^A \in \mathbb{R}^{pN^V \times \tilde{n}_p^K}, \quad \mathbf{D}^B \in \mathbb{R}^{N^V \times \tilde{n}_p^K}, \quad \mathbf{D}^C \in \mathbb{R}^{n_{p-2}^K \times \tilde{n}_p^K},$$

so that the matrix $\mathbf{D} \in \mathbb{R}^{\tilde{N}^K \times \tilde{n}_p^K}$ is given by

$$\begin{bmatrix} \mathbf{D}^A \\ \mathbf{D}^B \\ \mathbf{D}^C \end{bmatrix}.$$

The matrix \mathbf{D}^A represents the contributions of the standard edge basis functions; \mathbf{D}^B the contributions of the special edge functions; \mathbf{D}^C the contributions of the bulk functions.

Given φ_i an edge basis function, let $e(i)$ the edge, where φ_i has a nonzero moment. If φ_i is associated with the standard polynomial moments, then denote the nonzero order moment by $\beta(i)$. Recalling the definition of the edge moments (22), we set

$$\begin{aligned} \mathbf{D}_{i,\alpha}^A &= \frac{1}{|e(i)|} (\mathbb{L}_{\beta(i)}^{e(i)}, \tilde{m}_{\alpha|e(i)}^K)_{0,e(i)} \quad \forall i = 1, \dots, pN^V, \forall \alpha = 1, \dots, \tilde{n}_p^K, \\ \mathbf{D}_{i,\alpha}^B &= (\mathbf{n}_e \cdot \nabla \mathcal{S}_{\mathbf{A}}^{e(i)}, \tilde{m}_{\alpha|e(i)}^K)_{0,e(i)} \quad \forall i = 1, \dots, N^V, \forall \alpha = 1, \dots, \tilde{n}_p^K. \end{aligned}$$

As for the matrix \mathbf{D}^C , we simply write

$$\mathbf{D}_{i,\alpha}^C = \frac{1}{|K|} \int_K m_i^K \tilde{m}_\alpha^K \quad \forall i = 1, \dots, n_{p-2}^K, \forall \alpha = 1, \dots, \tilde{n}_p^K. \quad (64)$$

All the entries of the three matrices above can be computed exactly or approximated at any precision with a sufficiently accurate quadrature formula.

Remark 4. As for the computation of \mathbf{D}^C in (64) in the case $\tilde{m}_\alpha^K = \mathcal{S}_\mathbf{A}^K$, we suggest to use the following strategy. Given $m_i^K \in \mathbb{P}_{p-2}(K)$, it is possible to write

$$m_i^K = \Delta m_{p,i}^K$$

for some $m_{p,i}^K \in \mathbb{P}_p(K)$. We provide an explicit representation of $m_{p,i}^K$ in Appendix B.

Then, the integral in (64) can be rewritten using an integration by parts twice and the fact that $\Delta \mathcal{S}_\mathbf{A} = 0$ as

$$\frac{1}{|K|} \int_K m_i^K \mathcal{S}_\mathbf{A}^K = \frac{1}{|K|} \int_K \Delta m_{p,i}^K \mathcal{S}_\mathbf{A}^K = \frac{1}{|K|} \left[\int_{\partial K} \mathbf{n} \cdot \nabla m_{p,i}^K \mathcal{S}_\mathbf{A}^K - \int_{\partial K} m_{p,i}^K \mathbf{n} \cdot \nabla \mathcal{S}_\mathbf{A}^K \right].$$

■

Computation of the right-hand side. Proceed as in [11]: no enrichment involves the right-hand side.

Boundary conditions. We identify the boundary edge degrees of freedom of the discrete and exact solutions u_n and u . In other words, for all $e \in \mathcal{E}_n^B$ such that $e \subset \Gamma_D$, we impose the following condition:

$$\int_e (u_n - u) \tilde{m}_\alpha^e = 0 \quad \forall \alpha = 1, \dots, \dim(\tilde{\mathbb{P}}_{p-1}(e)).$$

The case of nonhomogeneous Neumann boundary conditions. Here, we address the implementation aspects for the computation of the Neumann boundary conditions term (34). In particular, given a canonical basis function φ_i associated with a nonzero moment on a Neumann edge $e \subset \Gamma_N$, we describe how to compute

$$\int_e g_N \tilde{\Pi}_{p-1}^{0,e} \varphi_i. \quad (65)$$

We can expand

$$\tilde{\Pi}_{p-1}^{0,e} \varphi_i = \sum_{\alpha=0}^{p-1} \lambda_\alpha^0 m_\alpha + \lambda_p^0 \mathcal{S}_\mathbf{A}^e. \quad (66)$$

Once we know the coefficients λ_α^0 , $\alpha = 0, \dots, p$, we are able to approximate the integral in (65) at any precision.

Define the matrix $\mathbf{G}^0 \in \mathbb{R}^{(p+1) \times (p+1)}$ and the vector $\mathbf{b}^0 \in \mathbb{R}^{p+1,1}$ as follows:

$$\mathbf{G}^0_{\alpha,\beta} := \begin{cases} \frac{2}{h_e} \frac{2}{2(\beta-1)+1} & \text{if } \alpha = \beta, \beta = 1, \dots, p \\ 0 & \text{if } \alpha \text{ is not equal to } \beta, \alpha, \beta = 1, \dots, p \\ (\mathcal{S}_\mathbf{A}^e, m_\beta)_{0,e} & \text{if } \alpha = p+1 \text{ and } \beta = 1, \dots, p; \beta = p+1 \text{ and } \alpha = 1, \dots, p \\ (\mathcal{S}_\mathbf{A}^e, \mathcal{S}_\mathbf{A}^e)_{0,e} & \text{if } \alpha = \beta = p+1. \end{cases}$$

Moreover, define the vector $\mathbf{b}^0 \in \mathbb{R}^{p+1,1}$ as the i -th column of the diagonal matrix $\mathbf{B}^0 \in \mathbb{R}^{(p+1) \times (p+1)}$, which is given by

$$\mathbf{B}^0_{\alpha,\beta} = \begin{cases} |e| & \text{if } \alpha = \beta \leq p \\ 1 & \text{if } \alpha = \beta = p+1 \end{cases}$$

The coefficients in (66) for the expansion of φ are computed solving the system

$$\mathbf{G}^0 \mathbf{\Lambda}^0 = \mathbf{b}^0.$$

In order to see this, it suffices to test (66) with the elements in a basis of $\tilde{\mathbb{P}}_{p-1}(e)$ and use the orthogonality property of the Legendre polynomials (63).

Remark 5. In the computation of the matrices \mathbf{B} , \mathbf{D} , \mathbf{G} , and the boundary conditions, the integrals involving singular functions are always boundary integrals. This fact is extremely relevant. Indeed, in order to compute integrals involving singular functions, we resort to Gauß-Jacobi quadrature formulas; see, e.g., [32, Section 4.8-1]. By doing so, the singular integrals can be computed up to machine precision with relatively few integration points, whereas the standard Gauß integration rule would need a disproportionate number of quadrature points in order to achieve the same precision. ■

Remark 6. The “ $G = BD$ ” test of [11, Remark 3.3] is valid also in the enriched framework. This is an excellent test to check the correctness of the implementation of the method. In order to fulfil this test correct, the integrals must be computed up to machine precision. Notably, we suggest to use suitable quadrature formulas. See Remark 5. ■

B Given a polynomial of degree p in two dimensions, how can we write it as the Laplacian of a polynomial of degree $p + 2$?

For all $p \in \mathbb{N}$, denote the set of the polynomials of degree ℓ in two dimensions by $\mathbb{P}_\ell(\mathbb{R}^2)$. When no confusion occurs, we replace $\mathbb{P}_p(\mathbb{R}^2)$ with \mathbb{P}_p .

In this appendix, we address the following question.

Question 1. Given $q_p \in \mathbb{P}_p$, is it possible to find $q_{p+2} \in \mathbb{P}_{p+2}$ in closed form such that $\Delta q_{p+2} = q_p$?

The answer to this question is crucial in the implementation of the method; see Remark 4.

It suffices to answer Question 1 for all q_p being the elements of a basis of \mathbb{P}_p . In fact, given $\{m_\alpha\}_{\alpha=1}^{\dim(\mathbb{P}_p)}$ a basis of \mathbb{P}_p , we can write

$$q_p = \sum_{\alpha=1}^{\dim(\mathbb{P}_p)} \lambda_\alpha m_\alpha, \quad \text{where } \lambda_\alpha \in \mathbb{R} \quad \forall \alpha = 1, \dots, \dim(\mathbb{P}_p).$$

Assume to know how to compute $\tilde{m}_\alpha \in \mathbb{P}_{p+2}$ such that $\Delta \tilde{m}_\alpha = m_\alpha$. Then, we have

$$\Delta q_{p+2} := \Delta \left(\sum_{\alpha=1}^{\dim(\mathbb{P}_p)} \lambda_\alpha \tilde{m}_\alpha \right) = \sum_{\alpha=1}^{\dim(\mathbb{P}_p)} \lambda_\alpha m_\alpha = q_p.$$

As a basis of \mathbb{P}_p , we will consider the basis of monomials. More precisely, given $p \in \mathbb{N}$, define the monomials of degree exactly equal to p as

$$m_s^{[p]} = x^{p+1-s} y^{s-1} \quad \forall s = 1, \dots, p+1,$$

and define the space of monomials of degree exactly equal to p as

$$\mathbb{M}_p := \text{span} \left\{ m_s^{[p]} \text{ with } s = 1, \dots, p+1 \right\}. \quad (67)$$

The main result reads as follows.

Theorem B.1. (i) Let $p \in \mathbb{N}$, $m_s^{[p]} = x^{p+1-s} y^{s-1} \in \mathbb{M}_p$ be such that $p+1 \geq 2s$, and $K_s \in \mathbb{N}$ be the largest integer such that $s - 2K_s \geq 1$. Then, the following identity is valid:

$$m_s^{[p]} = \sum_{k=0}^{K_s} \lambda_{s-2k}^{[p],s} \Delta m_{s-2k}^{[p+2]} \quad \forall s = 1, \dots, \left\lceil \frac{p+1}{2} \right\rceil. \quad (68)$$

The coefficients $\lambda_t^{[p],s}$ appearing in (68) are defined as follows: For all $s = 1, \dots, \left\lceil \frac{p+1}{2} \right\rceil$,

$$\lambda_{s-2k}^{[p],s} = (-1)^k \frac{1}{(p-s+3)(p-s+2)} \prod_{j=1}^k \frac{(s-1-2(j-1))(s-2-2(j-1))}{(p-s+3+2j)(p-s+2+2j)} \quad \forall k = 1, \dots, K_s.$$

We use the notation $\prod_{j=1}^0 \mu_j = 1$.
(ii) The following identity is valid:

$$m_{p+2-s}^{[p]} = \sum_{k=0}^{K_s} \lambda_{s-2k}^{[p],s} \Delta m_{p+4-s+2k}^{[p+2]} \quad \forall s = 1, \dots, \left\lfloor \frac{p+1}{2} \right\rfloor. \quad (69)$$

Proof. We only prove (i), for (ii) follows likewise.

The first two coefficients $\lambda_1^{[p],s}$ and $\lambda_2^{[p],s}$ can be computed by hand easily. As for the others, we proceed by induction. More precisely, given $s \geq 3$, assume that (68) is valid for monomials of the form $m_{\tilde{s}}^{[p]} = x^{p+1-\tilde{s}} y^{\tilde{s}-1}$ with $\tilde{s} \leq s$. We prove the assertion for the monomial $m_s^{[p]} = x^{p+1-s} y^{s-1}$.

Let $K_{s-2} \in \mathbb{N}$ be the largest integer such that $s-2-2K_{s-2} \geq 1$. Thanks to the induction hypothesis

$$m_{s-2}^{[p]} = \sum_{k=0}^{K_{s-2}} \lambda_{s-2-2k}^{[p],s-2} \Delta m_{s-2-2k}^{[p-2]},$$

we write

$$\begin{aligned} m_s^{[p]} &= x^{p+1-s} y^{s-1} \\ &= \frac{1}{(p+1-s+2)(p+1-s+1)} [\Delta(x^{p+1-s} y^{s-1}) - (s-1)(s-2)x^{p+1-s+2} y^{s-3}] \\ &= \frac{1}{(p-s+3)(p-s+2)} [\Delta(x^{p+1-s+2} y^s) - (s-1)(s-2)m_{s-2}^{[p]}] \\ &=: \frac{1}{(p-s+3)(p-s+2)} \Delta(x^{p+1-s+2} y^s) - \frac{(s-1)(s-2)}{(p-s+3)(p-s+2)} \sum_{k=0}^{K_{s-2}} \lambda_{s-2-2k}^{[p],s-2} \Delta m_{s-2-2k}^{[p+2]}. \end{aligned} \quad (70)$$

We prove that the coefficients on the right-hand side of (70) are those given in the assertion of the theorem: They must be equal to $\lambda_{s-2k}^{[p],s}$ for all $k = 0, \dots, K_s$.

On the one hand, we have that the coefficient associated with $\Delta(x^{p+1-s+2} y^{s-1})$ is

$$\frac{1}{(p-s+3)(p-s+2)},$$

which is nothing but $\lambda_{s-2k}^{[p],s}$.

As for the other coefficients, we have to show that

$$-\frac{(s-1)(s-2)}{(p-s+3)(p-s+2)} \lambda_{s-2-2k}^{[p],s-2} = \lambda_{s-2(k+1)}^{[p],s} \quad \forall k = 0, \dots, K_{s-2}.$$

To this purpose, for all $k = 0, \dots, K_{s-2}$, we observe that

$$\begin{aligned} &-\frac{(s-1)(s-2)}{(p-s+3)(p-s+2)} \lambda_{s-2-2k}^{[p],s-2} \\ &= -\frac{(s-1)(s-2)}{(p-s+3)(p-s+2)} (-1)^k \frac{1}{(p-(s-2)+3)(p-(s-2)+2)} \times \\ &\quad \times \prod_{j=1}^k \frac{((s-2)-1-2(j-1))((s-2)-2-2(j-1))}{(p-(s-2)+3+2j)(p-(s-2)+2+2j)} \\ &= (-1)^{k+1} \frac{1}{(p-s+3)(p-s+2)} \prod_{j=1}^{k+1} \frac{(s-1-2(j-1))(s-2-2(j-1))}{(p-s+3+2j)(p-s+2+2j)} = \lambda_{s-2(k+1)}^{[p],s}, \end{aligned}$$

whence the assertion follows. \square

An immediate consequence of Theorem B.1 is the following well known result.

Corollary B.2. *For all $p \in \mathbb{N}$, the Laplace operator Δ is surjective from $\mathbb{P}_{p+2}(\mathbb{R}^2)$ into $\mathbb{P}_p(\mathbb{R}^2)$.*

Next, we present a MatLab script that, given the degree of \mathbb{M}_p defined in (67), allows us to compute the coefficients in the expansion (68). The script can be found in Algorithm 1.

The output of the script consists of two matrices. The first matrix contains the coefficients of the expansion of $x^n y^m$, $n \geq m$, in terms of the Laplacian of monomials of the form $x^{\tilde{n}+2} y^{\tilde{m}}$, with $\tilde{n} \geq \tilde{m}$; the second matrix contains the coefficients of the expansion of $x^n y^m$, $m > n$, in terms of the Laplacian of monomials of the form $x^{\tilde{n}+2} y^{\tilde{m}}$, with $\tilde{m} = p + 2 - \tilde{n}, \dots, p + 2$.

Example B.1. Consider the case $p = 8$. The output of the script is provided by the two following matrices:

1/90	0	0	0	0
0	1/72	0	0	0
-2/(56 * 90)	0	1/56	0	0
0	-6/(42*72)	0	1/42	0
(12*2)/(30*56*90)	0	-12/(30*56)	0	1/30

and

1/42	0	-6/(42*72)	0
0	1/56	0	-2/(56 * 90)
0	0	1/72	0
0	0	0	1/90

Indeed, it can be checked that this is the correct output. In fact, we have

$$\begin{aligned}
x^8 &= \frac{1}{90} \Delta x^{10}, \\
x^7 y &= \frac{1}{72} \Delta x^9 y, \\
x^6 y^2 &= \frac{1}{56} \Delta x^8 y^2 - \frac{1}{56 * 90} \Delta x^8, \\
x^5 y^3 &= \frac{1}{42} \Delta x^7 y^3 - \frac{6}{42 * 72} \Delta x^7 y, \\
x^4 y^4 &= \frac{1}{30} \Delta x^6 y^4 - \frac{12}{30 * 56} \Delta x^8 y^2 + \frac{12 * 2}{30 * 56 * 90} \Delta x^8, \\
x^3 y^5 &= \frac{1}{42} \Delta x^3 y^7 - \frac{6}{42 * 72} \Delta y^8, \\
x^2 y^6 &= \frac{1}{56} \Delta x^2 y^8 - \frac{2}{56 * 90} \Delta x y^7, \\
x y^7 &= \frac{1}{72} \Delta x y^9, \\
y^8 &= \frac{1}{90} \Delta y^{10}.
\end{aligned}$$

References

- [1] P. F. Antonietti, G. Manzini, and M. Verani. The conforming virtual element method for polyharmonic problems. *Comput. Math. Appl.*, 79(7):2021–2034, 2020.
- [2] E. Artioli, L. Beirão Da Veiga, C. Lovadina, and E. Sacco. Arbitrary order 2D virtual elements for polygonal meshes: part I, elastic problem. *Comput. Mech.*, 60(3):355–377, 2017.
- [3] E. Artioli, S. De Miranda, C. Lovadina, and L. Patruno. A stress/displacement virtual element method for plane elasticity problems. *Comput. Methods Appl. Mech. Engrg.*, 325:155–174, 2017.
- [4] B. P. Ayuso de Dios, K. Lipnikov, and G. Manzini. The nonconforming virtual element method. *ESAIM Math. Model. Numer. Anal.*, 50(3):879–904, 2016.
- [5] I. Babuška and B. Q. Guo. Regularity of the solution of elliptic problems with piecewise analytic data. Part I. Boundary value problems for linear elliptic equation of second order. *SIAM J. Math. Anal.*, 19(1):172–203, 1988.
- [6] I. Babuška and B. Q. Guo. Regularity of the solution of elliptic problems with piecewise analytic data. Part II: The trace spaces and application to the boundary value problems with nonhomogeneous boundary conditions. *SIAM J. Math. Anal.*, 20(4):763–781, 1989.

- [7] I. Babuška and B.Q. Guo. The hp version of the finite element method for domains with curved boundaries. *SIAM J. Numer. Anal.*, 25(4):837–861, 1988.
- [8] I. Babuška and M. Suri. The hp version of the finite element method with quasiuniform meshes. *ESAIM Math. Model. Numer. Anal.*, 21(2):199–238, 1987.
- [9] L. Beirão da Veiga, C. Lovadina, and D. Mora. A virtual element method for elastic and inelastic problems on polytope meshes. *Comput. Methods Appl. Mech. Engrg.*, 295:327 – 346, 2015.
- [10] L. Beirão da Veiga, F. Brezzi, A. Cangiani, G. Manzini, L.D. Marini, and A. Russo. Basic principles of virtual element methods. *Math. Models Methods Appl. Sci.*, 23(01):199–214, 2013.
- [11] L. Beirão da Veiga, F. Brezzi, L.D. Marini, and A. Russo. The hitchhiker’s guide to the virtual element method. *Math. Models Methods Appl. Sci.*, 24(8):1541–1573, 2014.
- [12] L. Beirão da Veiga, A. Chernov, L. Mascotto, and A. Russo. Exponential convergence of the hp virtual element method with corner singularity. *Numer. Math.*, 138(3):581–613, 2018.
- [13] L. Beirão da Veiga, F. Dassi, and A. Russo. High-order virtual element method on polyhedral meshes. *Comput. Math. Appl.*, 74(5):1110–1122, 2017.
- [14] L. Beirão da Veiga, C. Lovadina, and A. Russo. Stability analysis for the virtual element method. *Math. Models Methods Appl. Sci.*, 27(13):2557–2594, 2017.
- [15] L. Beirão da Veiga, C. Lovadina, and G. Vacca. Divergence free virtual elements for the Stokes problem on polygonal meshes. *ESAIM Math. Model. Numer. Anal.*, 51(2):509–535, 2017.
- [16] E. Benvenuti, A. Chiozzi, G. Manzini, and N. Sukumar. Extended virtual element method for the Laplace problem with singularities and discontinuities. *Comput. Methods Appl. Mech. Engrg.*, 356:571–597, 2019.
- [17] S. C. Brenner and L. R. Scott. *The mathematical theory of Finite Element Methods*, volume 15. Texts in Applied Mathematics, Springer-Verlag, New York, third edition, 2008.
- [18] S. C. Brenner and L.-Y. Sung. Virtual element methods on meshes with small edges or faces. *Math. Models Methods Appl. Sci.*, 268(07):1291–1336, 2018.
- [19] A. Cangiani, E. H. Georgoulis, T. Pryer, and O. J. Sutton. A posteriori error estimates for the virtual element method. *Numer. Math.*, 137(4):857–893, 2017.
- [20] A. Cangiani, G. Manzini, and O. J. Sutton. Conforming and nonconforming virtual element methods for elliptic problems. *IMA J. Numer. Anal.*, 37(3):1317–1354, 2016.
- [21] S. Cao and L. Chen. Anisotropic error estimates of the linear virtual element method on polygonal meshes. *SIAM J. Numer. Anal.*, 56(5):2913–2939, 2018.
- [22] L. Chen and X. Huang. Nonconforming virtual element method for $2m$ -th order partial differential equations in \mathbb{R}^n . *Math. Comp.*, 89:1711–1744, 2020.
- [23] M. Costabel and M. Dauge. Crack singularities for general elliptic systems. *Math. Nachr.*, 235(1):29–49, 2002.
- [24] F. Dassi, C. Lovadina, and M. Visinoni. A three-dimensional Hellinger-Reissner virtual element method for linear elasticity problems. *Comput. Methods Appl. Mech. Engrg.*, 364, 2020.
- [25] E. Di Nezza, G. Palatucci, and E. Valdinoci. Hitchhiker’s guide to the fractional Sobolev spaces. *Bull. Sci. Math.*, 136(5):521–573, 2012.
- [26] P. Grisvard. *Elliptic problems in nonsmooth domains*. SIAM, 2011.
- [27] L. Mascotto. Ill-conditioning in the virtual element method: stabilizations and bases. *Numer. Methods Partial Differential Equations*, 34(4):1258–1281, 2018.
- [28] L. Mascotto, I. Perugia, and A. Pichler. Non-conforming harmonic virtual element method: h - and p -versions. *J. Sci. Comput.*, 77(3):1874–1908, 2018.
- [29] N. Moës and T. Belytschko. Extended finite element method for cohesive crack growth. *Engineering fracture mechanics*, 69(7):813–833, 2002.
- [30] N. Moës, J. Dolbow, and T. Belytschko. A finite element method for crack growth without remeshing. *Internat. J. Numer. Methods Engrg.*, 46(1):131–150, 1999.
- [31] I. Perugia, P. Pietra, and A. Russo. A plane wave virtual element method for the Helmholtz problem. *ESAIM Math. Model. Numer. Anal.*, 50(3):783–808, 2016.
- [32] A. Ralston and P. Rabinowitz. *A first course in numerical analysis*. Courier Corporation, 2001.
- [33] D. Schötzau, Ch. Schwab, and T. P. Wihler. hp -dGFEM for second-order elliptic problems in polyhedra I: Stability on geometric meshes. *SIAM J. Numer. Anal.*, 51(3):1610–1633, 2013.
- [34] C. Schwab. *p - and hp - Finite Element Methods: Theory and Applications in Solid and Fluid Mechanics*.
- [35] T. Strouboulis, I. Babuška, and K. Copps. The design and analysis of the generalized finite element method. *Comput. Methods Appl. Mech. Engrg.*, 181(1-3):43–69, 2000.
- [36] S. Weißer. *BEM-based Finite Element Approaches on Polytopal Meshes*, volume 130. Lecture Notes in Computational Science and Engineering, Springer, 2019.
- [37] P. Wriggers, B. D. Reddy, W. Rust, and B. Hudobivnik. Efficient virtual element formulations for compressible and incompressible finite deformations. *Comput. Mech.*, 60(2):253–268, 2017.

Algorithm 1 Computing the coefficients in the expansions (68) and (69).

```
function [M_x,M_y]=polynomial_laplacian(p)
%%
if ceil(p/2)==p/2
    dim_M=ceil(p/2)+1;
else
    dim_M=ceil(p/2);
end
%%
M=zeros(dim_M,dim_M);
%%
for n=1:dim_M
    M(n,n) = 1/((p+2-(n-1))*(p+1-(n-1)));
    for m=n-2:-2:1
        M(n,m)=-((n-1)*(n-2))/((p+2-(n-1))*(p+1-(n-1))) * M(n-2,m);
    end
end
%%
M_x = M;
if ceil(p/2)==p/2
    M_y = fliplr(flipud(M(1:end-1,1:end-1)));
else
    M_y = fliplr(flipud(M));
end
%%
return
```
